°C; ^{1}H NMR (CD_3CN) δ 3.50 (s, 3 H), 5.30 (q, 2 H, $\Delta\nu_{AB}$ = 21.0 Hz). Anal. Calcd for $C_{23}H_{17}F_3N_2O_3S_2$: C, 56.3; H, 3.5; N, 5.7. Found: C, 56.9; H, 3.6; N, 5.9.

Phenylmethyl(*m*-cyanobenzyl)sulfonium Tetrafluoroborate. Thioanisole (8.05 mmol, 1.00 g, Aldrich), α-bromo-*m*-tolunitrile (8.05 mmol, 1.57 g, Aldrich), and silver tetrafluoroborate (8.05 mmol, 1.57 g, Aldrich) were added to 30 mL of dry methylene chloride, and the mixture was stirred at room temperature for 20 h. The reaction mixture was filtered and flash evaporated to dryness, and attempted crystallization from acetonitrile/diethyl ether gave the product as a colorless oil [2.5 g (95% yield)]: ^{1}H NMR (CH_3CN) δ 3.22 (s, 3 H), 4.70 (q, 2 H, $\Delta\nu_{AB}$ = 15.6 Hz); mass spectrum (FDMS), *m/e* 240 (M^+).

The $\{[(CH_3)_5C_5]Rh(cis\text{-}Nb_2W_4O_{19})\}^{2-}$ Isomers: Synthesis, Structure, and Dynamics

C. J. Besecker,[1a] V. W. Day,*[1b,c] W. G. Klemperer,*[1a] and M. R. Thompson[1c]

Contribution from the School of Chemical Sciences, University of Illinois, Urbana, Illinois 61801, the Department of Chemistry, Columbia University, New York, New York 10027, the Crystalytics Company, Lincoln, Nebraska 68501, and the Department of Chemistry, University of Nebraska, Lincoln, Nebraska 68588.
Received November 16, 1983

Abstract: The *cis*-$Nb_2W_4O_{19}^{4-}$ anion reacts with $\{[(CH_3)_5C_5]RhCl_2\}_2$ in CH_2Cl_2 to form the title complex. According to a single-crystal X-ray diffraction study, the *cis*-$Nb_2W_4O_{19}^{4-}$ ion behaves as a tridentate ligand in this complex, utilizing three contiguous bridging oxygen atoms for the rhodium binding site. Of the three diastereomers possible for this adduct, only two are formed under the reaction conditions. The third diastereomer is formed from a mixture of these two in CH_3NO_2 at room temperature in the presence of a catalyst, solvated $[(CH_3)_5C_5]Rh^{2+}$. Employing the results of ^{1}H and ^{17}O NMR spectroscopic studies, mechanisms are proposed for the formation and isomerization of $\{[(CH_3)_5C_5]Rh(Nb_2W_4O_{19})\}^{2-}$. The former involves the intermediate $\{[(CH_3)_5C_5]RhCl_2(Nb_2W_4O_{19})\}^{4-}$; the latter involves the $\{[(CH_3)_5C_5]Rh\}_2(Nb_2W_4O_{19})$ molecule as an intermediate.

The *cis*-$Nb_2W_4O_{19}^{4-}$ anion[2-5] has a structure tailor-made for systematically examining the reaction chemistry of small, closed-packed oxygen surfaces. Its 19 oxygen atoms form the octahedral, cubic close-packed array shown in the space-filling representation a.[6] The six d^0 Nb^V and W^{VI} centers occupy octahedral interstices within this array, and they are themselves arranged in the cis-octahedral fashion illustrated in b.

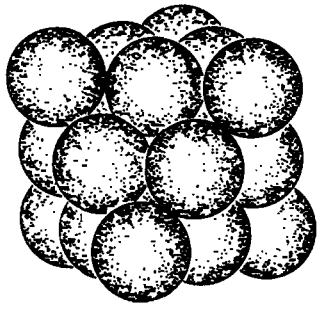

a

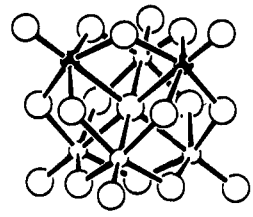

b

The $Nb_2W_4O_{19}^{4-}$ anion is sufficiently basic to form air-stable metal tricarbonyl adducts $[(OC)_3M(cis\text{-}Nb_2W_4O_{19})]^{3-}$, M = Mn[1] and Re[1,5] In these complexes, the polyoxoanion behaves as a tridentate ligand, utilizing a triangle of bridging oxygen atoms as the metal tricarbonyl binding site. Three diastereomers c–e are possible for this structure, and low-resolution 13.5-MHz ^{17}O NMR spectroscopy has shown that isomer d predominates for the M = Re complex.[5]

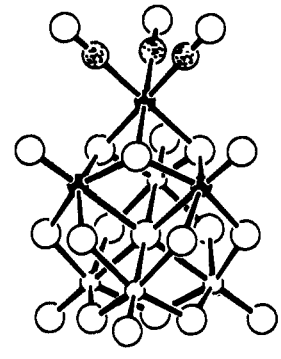

c

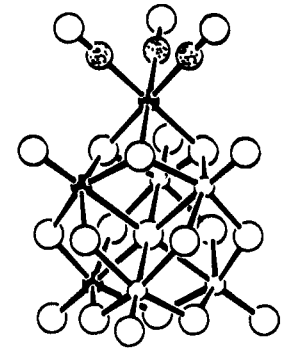

d

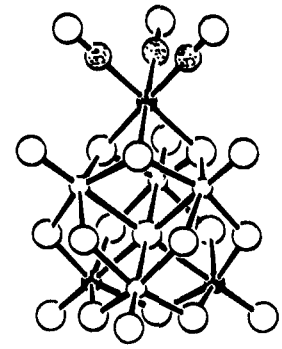

e

Simple electrostatic considerations would dictate that $M(CO)_3^+$ cations prefer $Nb_2W_4O_{19}^{4-}$ binding sites adjacent to pentavalent

(1) (a) University of Illinois (current address) and Columbia University. (b) Crystalytics Company. (c) University of Nebraska.
(2) Dabbabi, M.; Boyer, M. *J. Inorg. Nucl. Chem.* **1976**, *38*, 1011–14.
(3) Rocchiccioli-Deltcheff, C.; Thouvenot, R.; Dabbabi, M. *Spectrochim. Acta, Part A* **1977**, *33A*, 143–53.
(4) Dabbabi, M.; Boyer, M.; Launay, J.-P.; Jeannin, Y. *J. Electroanal. Chem.* **1977**, *76*, 153–64.
(5) Besecker, C. J.; Klemperer, W. G. *J. Am. Chem. Soc.* **1980**, *102*, 7598–7600.
(6) M_6O_{19} units were drawn using O_h-idealized $W_6O_{19}^{2-}$ coordinates;[7] $[(CH_3)_5C_5]$ units were drawn using D_{5h}-idealized coordinates with 1.43 Å ring carbon–ring carbon distances and 1.51-Å methyl carbon–ring carbon distances.[8] Rhodium–oxygen and rhodium–carbon bond lengths were fixed at 2.20 and 2.16 Å, respectively. Van der Waals radii[9] for oxygen (1.4 Å), carbon (1.7 Å), chlorine (1.8 Å), and methyl groups (2.0 Å) were used for space-filling drawings.

0002-7863/84/1506-4125$01.50/0

Nb^V as opposed to hexavalent W^{VI} centers. We were therefore surprised by the apparent stability of isomer d relative to isomer c, and we remeasured the ^{17}O NMR spectra of $[(OC)_3M(cis\text{-}Nb_2W_4O_{19})]^{3-}$ at 33.9 MHz.[10] Although both isomers c and e were detected in these spectra, we were unable to carry out quantitative studies which might establish the kinetic and thermodynamic factors influencing isomer distributions. Since an understanding of these factors might in turn yield insight into the relative nucleophilicities and basicities of $Nb_2W_4O_{19}^{4-}$ surface oxygens, we decided to investigate the binding site preferences of an analogous d^6 metal hydrocarbyl unit which might be more amenable to quantitative studying using ^1H NMR spectroscopy. We report here the results of such an investigation of the $\{[(CH_3)_5C_5]Rh(cis\text{-}Nb_2W_4O_{19})\}^{2-}$ system.

Experimental Section

Reagents, Solvents, and General Procedures. The following were purchased from commercial sources and used without further purification: $Na_2WO_4\cdot 2H_2O$ and glacial acetic acid (Fisher); 30% aqueous H_2O_2 and 85% hydrated KOH pellets (Mallinckrodt); $RhCl_3\cdot xH_2O$ and $AgPF_6$ (Strem); CD_3NO_2, CD_2Cl_2, Nb_2O_5, and hexamethylbicyclo[2.2.0]hexadiene (Aldrich); $(CH_3)_4NBr$ and 0.4 M aqueous $(n\text{-}C_4H_9)_4NOH$ (Eastman); $Na_2S_2O_4\cdot 2H_2O$ and Na_2SO_4 (Amend); 50–100 mesh sulfonated 2% cross-linked polystyrene cation exchange resin in hydrogen form (Bio-Rad); and ^{17}O-enriched water (Monsanto Research).

$K_7HNb_6O_{19}\cdot 13H_2O$ was prepared according to literature procedures.[11,12] Experience showed that well-formed crystalline product was obtained reproducibly only if deionized water was employed, and this water was degassed by vigorous boiling for 15 min immediately before use. $(Nb_2W_4O_{19})Na_2[(CH_3)_4N]_2$ was prepared according to literature procedures[2] and used in subsequent reactions as the crude, ethanol-precipitated product. $\{[(CH_3)_5C_5]RhCl_2\}_2$ was prepared as described in ref 13. Cation exchange resin was converted quantitatively from H^+ to $(n\text{-}C_4H_9)_4N^+$ form after being stirred with 20% molar excess $(n\text{-}C_4H_9)$-NOH as a 0.1 M aqueous solution for 24 h. Resin capacity (mmol/g) was determined from H^+ resin with use of standard procedures;[14] percentage cation exchange was determined by back titration of unreacted $(n\text{-}C_4H_9)_4NOH$.

Anhydrous diethyl ether (Mallinckrodt) was used only from freshly opened cans. Acetonitrile (Aldrich, 99%) and dichloromethane (Fisher) were distilled under N_2 from P_4O_{10} onto activated 3 Å molecular sieves. Chloroform, 1,2-dichloroethane, and toluene (all Fisher) were stored over activated 4 Å molecular sieves. Solvents used for the preparation of ^{17}O-enriched samples were purified more thoroughly and used within 48 h after distillation. Prepurified acetonitrile and dichloromethane were distilled under N_2 from CaH_2. The middle fractions were collected and stored over activated 3 Å molecular sieves. Chloroform was distilled under N_2 from P_4O_{10} onto activated 3 Å molecular sieves. Molecular sieves were activated by drying at 350 °C for 24 h and storing under N_2 at room temperature.

Reactions involving rhodium reagents were routinely performed in an N_2 atmosphere. All manipulations of ^{17}O-enriched materials were performed in closed systems with vigorous exclusion of atmospheric moisture to avoid isotopic dilution.

Analytical Procedures. Elemental analyses were performed by Galbraith Laboratories, Knoxville, TN. Infrared spectra were measured from mineral oil (Nujol) mulls between NaCl plates on a Perkin-Elmer 1330 spectrometer and were referenced to the 1028-cm^{-1} band of a 0.05-mm polystyrene film. ^1H and ^{13}C NMR spectra were recorded, 360 and 90.5 MHz, respectively, on a Nicolet NTC-360 spectrometer equipped with a deuterium lock. Chemical shifts were internally referenced to $(CH_3)_4Si$. ^{183}W and ^{17}O NMR spectra were measured on an unlocked FTNMR system equipped with a 5.87-T Oxford Instruments magnet and a Nicolet NIC-80 data system.

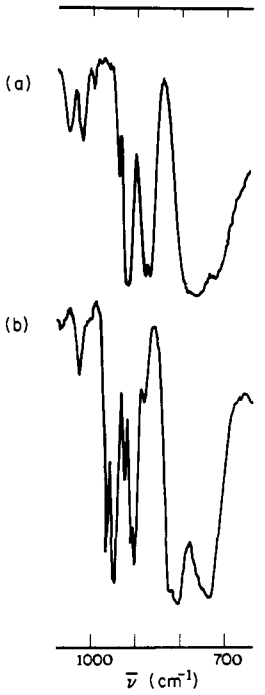

Figure 1. IR spectra of (a) $(Nb_2W_4O_{19})[(n\text{-}C_4H_9)_4N]_4$ and (b) $\{[(CH_3)_5C_5]Rh(Nb_2W_4O_{19})\}[(n\text{-}C_4H_9)_4N]_2$ measured from Nujol mulls. See Experimental Section for numerical data.

Tungsten-183 FTNMR spectra were measured at 10.4 MHz in 20-mm diameter sideways-spinning sample tubes (8-mL sample volume) and were referenced to 2.0 M aqueous Na_2WO_4 contained in a concentric 5-mm sample tube (0.4-mL volume). The spectra were recorded over a 3000-Hz bandwidth by using a 24-μs pulse width and at a 0.31-Hz pulse repetition rate. Spectra were digitized by using 16 384 data points; i.e., digital resolution of 0.18 Hz/data point was obtained.

Oxygen-17 FTNMR spectra were measured from CH_3CN solutions in 12-mm, vertical sample tubes without sample spinning and were referenced to 25 °C tap water with use of the sample replacement method. The pulse repetition rate was 5.88 Hz; a spectral bandwidth of 50 000 Hz was digitized by using 8192 data points. The pulse width employed, 16 μs, corresponded to a 45° pulse. The errors associated with ^{17}O chemical shift values are ±3 ppm for line widths <200 Hz, ±5 ppm for line widths >200 but <400 Hz, and ±7 ppm for line widths >400 Hz. All reported widths have been corrected for exponential line broadening. The errors associated with line width values are ±20 Hz for line widths <100 Hz, ±40 Hz for line widths >100 but <400 Hz, and ±60 Hz for line widths >400 Hz.

Chemical shifts for all nuclei are reported as positive numbers for resonances that are observed at higher frequency (lower field) than the appropriate reference.

Preparation of $(Nb_2W_4O_{19})[(n\text{-}C_4H_9)_4N]_4$. A solution prepared from 18.7 g (13.2 mmol) of $(Nb_2W_4O_{19})Na_2[(CH_3)_4N]_2$ and 1 L of deionized water was passed at a flow rate of ca. 2 mL/min through a 2-cm-diameter column containing 60 mmol of $(n\text{-}C_4H_9)_4N^+$ cation on the exchange resin described above which had been prewashed with 100 mL of deionized water. The initial 50-mL effluent was discarded and the remainder combined with effluent generated by rinsing the column with 50 mL of deionized water after elution was completed. The effluent was evaporated to an oily solid under vacuum at 40–50 °C and washed with 3 × 50 mL of ether to yield a tacky, off-white solid which was dried overnight in vacuo over P_4O_{10}. The crude product was dissolved in 75 mL of $1,2\text{-}C_2H_4Cl_2$ and gravity filtered under N_2 to remove insoluble impurities. Addition of excess ether (400 mL) to the filtrate caused separation of a tacky solid or oil which solidified to an off-white powder upon washing with 3 × 100 mL of ether and scratching with a spatula. The solid was collected by suction filtration, washed with 3 × 50 mL of ether, and dried in vacuo over P_4O_{10} to yield 21.1 g of crude product (9.6 mmol, 73% based on Nb). At this stage the product is quite pure and suitable for use in subsequent reactions. It may be crystallized by dissolving 3.0 g of compound in 9 mL of $CHCl_3$, filtering if necessary, and cooling to −30 °C. After 12 h small, colorless crystals appear which may be collected by suction filtration, washed with 3 × 20 ml ether, and dried in vacuo over P_4O_{10} to yield 2.1 g of a slightly hygroscopic, air-stable, colorless solid. The analytical sample was recrystallized three times.

(7) Fuchs, J.; Freiwald, W.; Hartl, H. *Acta Crystallogr., Sect. B* **1978**, *B34*, 1764–70.
(8) Churchill, M. R.; Julis, S. A.; Rotella, F. J. *Inorg. Chem.* **1977**, *16*, 1137–41.
(9) Pauling, L. "The Nature of the Chemical Bond"; 3rd ed.; Cornell University Press: Ithaca, New York, 1960; p 260.
(10) Besecker, C. J.; Day, V W.; Klemperer, W. G.; Thompson, M. R., submitted for publication.
(11) Filowitz, M.; Ho, R. K. C.; Klemperer, W. G.; Shum, W. *Inorg. Chem.* **1979**, *18*, 93–103.
(12) Flynn, C. M., Jr.; Stucky, G. D. *Inorg. Chem.* **1969**, *8*, 178–80.
(13) Kang, J. W.; Moseley, K.; Maitlis, P. M. *J. Am. Chem. Soc.* **1969**, *91*, 5970–7.
(14) Vogel, A. "A Textbook of Quantitative Inorganic Analysis"; 4th ed.; revised by Bassett, J.; Denney, R. C.; Jeffrey, G. H.; Mendham, J.; Longman: New York, 1978; pp 180–1.

Anal. Calcd for $C_{64}H_{144}N_4Nb_2W_4O_{19}$: C, 35.02; H, 6.61; N, 2.55; Nb, 8.46; W, 33.50. Found: C, 34.95; H, 6.67; N, 2.47; Nb, 8.36; W, 33.62. IR (Nujol, 700–1000 cm^{-1}, see Figure 1a): 733 (sh, br), 783 (s, br), 880 (s), 892 (s), 927 (s), 950 (m) cm^{-1}; cf. ref 3. ^{17}O NMR (0.08 M; 75 °C; 10 atom % ^{17}O; 20 000 acquisitions; preacquisition delay time = 50 μs; 0-Hz exponential line broadening): δ 754 (321-Hz line width, ONb), 691 (68, OW), 491 (282, ONb_2), 435 (114, ONbW), 375 (71, OW_2), −48 (17, ONb_2W_4); ^{17}O NMR (under the same conditions as above but at 27 °C): δ 752 (305-Hz line width, ONb), 691 (120, OW), 491 (153, ONb_2), 434 (88, ONbW), 373 (130, OW_2), −51 (9, ONb_2W_4). ^{183}W NMR (CH_3CN, 25 °C, 0.33 M): δ 80.3, 47.7; $^2J_{WW}$ = 5.5 Hz.

Oxygen-17 Enrichment of $(Nb_2W_4O_{19})[(n\text{-}C_4H_9)_4N]_4$. A 20-mL vial containing a magnetic stirring bar was charged with 1.90 g of recrystallized $(Nb_2W_4O_{19})[(n\text{-}C_4H_9)_4N]_4$, 0.43 mL of 0.4 M $(n\text{-}C_4H_9)_4NOH$, and 8.85 mL of ^{17}O-enriched water. The vial was capped and immersed to the level of the liquid in a 95 ± 5 °C oil bath. The slurry was stirred at this temperature for 13 h and cooled to room temperature. It was then transferred by pipet to a 25-mL round-bottom flask and attached to a vacuum line. After 4 freeze–pump–thaw degassing cycles, the slurry was frozen and the enriched water recovered by vacuum sublimation at room temperature into a receiving flask maintained at liquid-nitrogen temperature. The resulting solid was washed with 3 × 10 mL of ether and dried overnight in vacuo over P_4O_{10}. The crude product was then dissolved into 7.5 mL of $CHCl_3$, the resulting suspension gravity filtered to remove insoluble decomposition products, and the filtrate cooled to −30 °C. Crystals which separated after 4 h were collected, washed with ether, and dried in vacuo. Yields varied from 40 to 70%.

Preparation of $\{[(CH_3)_5C_5]Rh(Nb_2W_4O_{19})\}[(n\text{-}C_4H_9)_4N]_2$, Two-Diastereomer Mixture. A solution of 0.106 g (0.17 mmol) of $\{[(CH_3)_5C_5]RhCl_2\}_2$ in 12 mL of CH_2Cl_2 was added dropwise over a 3–5 min period to a rapidly stirred solution of $(Nb_2W_4O_{19})[(n\text{-}C_4H_9)_4N]_4$ (0.75 g, 0.34 mmol) in 2 mL of CH_2Cl_2. During this addition, the product began to precipitate from solution as an orange powder. Stirring was continued for 10 min after the addition was complete, and the powder was then collected by filtration, washed with 3 × 5 mL of CH_2Cl_2 and 3 × 5 mL of ether, and dried in vacuo over P_4O_{10} (0.50 g, 0.26 mmol, 75%). Crystalline material was obtained by dissolving this crude product in ca. 17 mL of boiling CH_3CN, gravity filtering to remove insoluble solids, and reducing the volume of the clear, orange filtrate to 13 mL by boiling off solvent. The small block-shaped crystals which formed after cooling to 25 °C were collected, washed with ether, and dried in vacuo, yielding 0.37 g (0.19 mmol, 74%) powder. This crystallization procedure leads to formation of the third diastereomer in small quantities. The analytical sample was crystallized three times. Anal. Calcd for $C_{42}H_{87}N_2RhNb_2W_4O_{19}$: C, 25.89; H, 4.50; N, 1.44; Rh, 5.28; Nb, 9.54; W, 37.75. Found: C, 25.85; H, 4.44; N, 1.51; Rh, 5.19; Nb, 9.70; W, 37.52. IR (Nujol, 700–1000 cm^{-1}, see Figure 1b): 736 (s, br), 805 (s, br), 825 (sh, br), 880 (w), 902 (s), 913 (s), 926 (m), 943 (sh), 949 (s), 965 (s), 971 (sh) cm^{-1}. ^1H NMR: in addition to cation resonances at δ 3.32–3.22, 1.78–1.68, 1.48–1.38, and 1.0–0.95, two $(CH_3)_5C_5$ singlets are observed at δ 1.95 and 1.91 in CD_3NO_2 at 25 °C. These singlets are observed at δ 1.94 and 1.91 in CD_2Cl_2 at 25 °C but appear at δ 1.91 and 1.86 in CD_2Cl_2 at −20 °C. ^{17}O NMR (2.2 × 10^{-3} M; 25 °C; 51 atom % ^{17}O; 263 000 acquisitions; preacquisition delay time = 125 μs; 10-Hz exponential line broadening): see Table I.

Preparation of $\{[(CH_3)_5C_5]Rh(Nb_2W_4O_{19})\}[(n\text{-}C_4H_9)_4N]_2$, Three-Diastereomer Mixture. Since $AgPF_6$ is quite hygroscopic, this preparation was carried out in an anhydrous environment. A solution of 0.43 g (1.7 mmol) of $AgPF_6$ in 10 mL of CH_3CN was added with stirring to a slurry of 0.265 g (0.43 mmol) of $\{[(CH_3)_5C_5]RhCl_2\}_2$ in 11 mL of CH_3CN. A rapid, exothermic reaction occurred, resulting in immediate precipitation of AgCl and generation of $\{[(CH_3)_5C_5]Rh(NCCH_3)_3\}^{2+}$.[15] The AgCl was gravity filtered off and washed with 3 × 0.5 mL of CH_3CN. These washes were added to the clear orange filtrate, and the combined solution was added with stirring to a solution of 1.88 g (0.86 mmol) of $(Nb_2W_4O_{19})[(n\text{-}C_4H_9)_4N]_4$ in 11 mL of CH_2Cl_2. During this addition or shortly thereafter, product began to precipitate from the reaction mixture as an orange powder. After 10 min of continued stirring, excess ether (50 mL) was added to complete product precipitation. The orange powder was collected by suction filtration, washed with 3 × 5 mL of CH_2Cl_2 and 3 × 5 mL of ether, and dried in vacuo over P_4O_{10} (1.55 g, 0.80 mmol, 93% yield). Crystallization was accomplished as described above for the two-diastereomer mixture. The IR spectrum of this material is indistinguishable from that of the two-diastereomer mixture described above. Its ^1H NMR at 25 °C in CD_3NO_2 differs only by the presence of a third $(CH_3)_5C_5$ resonance at δ 1.86. $^{13}C\{^1H\}$ NMR: (CD_3NO_2, 25 °C, 0.1 M $Cr(acac)_3$): δ 96.1 (d, $^1J_{CRh}$ = 10 Hz), 95.4 (d, $^1J_{CRh}$ = 10 Hz), and 94.9 (d, $^1J_{CRh}$ = 10 Hz) [$(CH_3)_5C_5$], 59.7 (s, NCH_2),[16] 24.6 (s, NCH_2CH_2),[16] 20.5 (s, CH_2CH_3),[16] 13.8 (s, CH_2CH_3),[16] 9.1 [$(CH_3)_5C_5$]. ^{17}O NMR (8.0 × 10^{-3} M; 79 °C; 41 atom % ^{17}O; 450 000 acquisitions; preacquisition delay time = 100 μs; 5-Hz exponential line broadening): see Table I.

X-ray Crystallographic Study[17] of $\{[(CH_3)_5C_5]Rh(Nb_2W_4O_{19})\}[(n\text{-}C_4H_9)_4N]_2$. Large well-shaped single crystals of $\{[(CH_3)_5C_5]Rh(Nb_2W_4O_{19})\}[(n\text{-}C_4H_9)_4N]_2$ (**1**), obtained as a three-diastereomer mixture from CH_3CN solution as described above, were suitable for X-ray diffraction studies. The crystals are, at 20 ± 1 °C, triclinic with a = 11.081 (3) Å, b = 11.773 (3) Å, c = 12.444 (4) Å, α = 115.85 (2)°, β = 99.30 (2)°, γ = 80.57 (2)°, V = 1434 (1) Å^3, and Z = 1 (μ_a(Mo Kᾱ)[18a] = 8.88 mm^{-1}; d_{calcd} = 2.256 g cm^{-3}). Having verified the absence of higher symmetry for this lattice by means of a Delauney reduction and experimentally determined the density of the crystals to be 2.24 g cm^{-3}, the choice of space groups was either noncentrosymmetric $P1\text{–}C_1^1$ (No. 1)[19a] with no crystallographically imposed molecular symmetry or centrosymmetric $P\bar{1}\text{–}C_i^1$ (No. 2)[19b] with the anion possessing C_i symmetry. With space group $P1$ being relatively rare for (racemic) synthetic compounds, two other possibilities appeared to remain: the crystal did not contain a $\{[(CH_3)_5C_5]Rh(Nb_2W_4O_{19})\}^{2-}$ anion or it was disordered in the lattice about a crystallographic inversion center. After verifying the above lattice constants from nearly a dozen different crystals from several different preparations of **1** and checking the analytical and spectroscopic data for **1** it was decided to proceed with the structure determination.

Intensity measurements were made on a Nicolet $P\bar{1}$ autodiffractometer using 1.00° wide ω scans and graphite-monochromated Mo Kᾱ radiation for a parallelepiped-shaped specimen having dimensions of 0.23 × 0.25 × 0.38 mm. This crystal was glued with epoxy to the end of a thin glass fiber with a tip diameter of 0.18 mm and mounted on a goniometer with

Table I. 33.9-MHz ^{17}O NMR Spectral Data for Compound **1** as a Mixture of Two and Three Diastereomers[a]

assignment[b]	two-diastereomer mixture, 25 °C[c]	three-diastereomer mixture, 79 °C[c]
$ORhW_2$	99 (78)	99 (71) 104 (71)
ORhNbW	151 (313)	147 151 } (336[d])
$ORhNb_2$	199 (497)	199 (576)
OW_2	389 (55) 394 (53) 403 (69) 407[e] 409 (66)	390 (52) 392[e] 395 (49) 403 (63) 409[e] 411 (63)
ONbW	453 (256) 460[e,f] 467 (141)	454 461 } (750[d]) 468
ONb_2	514 (370)	515 (526)
OW	731 (115) 738 741 } (175)[d]	731[e] 733[e,f] 735[e] 738[e] 741[e] 742[e,f]
ONb	801 (479)	802 (710)

[a] Spectra are shown in Figures 6 and 7; information regarding sampreparation, spectral acquisition, and error margins is given in the erimental Section. [b] As discussed in the text, a given oxygen environment is identified by the number and type of metal atoms an oxygen is bonded to. [c] Chemical shifts in ppm are followed by line widths, fwhm unless indicated otherwise, in Hz. [d] Combined line width of the bracketed resonances measured at half-maximum of the most intense peak. [e] Line width could not be measured. See Figure 6 or 7. [f] Shoulder.

(15) White, C.; Thompson, S. J.; Maitlis, P. M. *J. Chem. Soc., Dalton Trans.* **1977**, 1654–61.

(16) Hart, D. J.; Ford, W. T. *J. Org. Chem.* **1974**, *39*, 363–6.

(17) See paragraph at end of paper regarding supplementary material.

(18) "International Tables for X-Ray Crystallography"; Kynoch Press: Birmingham, England, 1974; Vol. IV, (a) pp 55–66, (b) pp 99–101, (c) pp 149–50.

(19) "International Tables for X-Ray Crystallography"; Kynoch Press: Birmingham, England, 1969; Vol. I, (a) p 74, (b) p 75.

its longest dimension nearly parallel to the φ axis of the diffractometer. Data were collected by using the ω-scanning technique with a normal-focus X-ray tube and a 4° take-off angle. For those reflections having $2\theta_{\text{Mo K}\bar{\alpha}} < 42.90°$, a scanning rate of 6 deg/min was employed for a scan between ω settings 0.50° above and below the calculated K$\bar{\alpha}$ (λ = 0.71073 Å) doublet value for each reflection. A scanning rate of 4 deg/min was employed for the remaining reflections. Counts were accumulated for 19 equal time intervals during each scan and those 13 contiguous intervals that had the highest single accumulated count at their midpoint were used to calculate the net intensity from scanning. A careful and systematic preliminary study of peak widths (half-height to half-height) indicated little variation from a value of 0.32° in ω for various orientations of the crystal. Background counts, each lasting one-fourth of the total scan time used for the net intensity scan, were measured at ω settings 0.50° above and below the calculated value for each reflection. A total of 6256 independent reflections having $2\theta_{\text{Mo K}\bar{\alpha}} < 54.90°$ (the equivalent of 1.0 limiting Cu K$\bar{\alpha}$ spheres) were measured in two concentric shells of increasing 2θ containing approximately 3125 reflections each. The six standard reflections measured every 300 reflections as a monitor for possible disalignment and/or deterioration of the crystal gave no indication of either. The intensity data were corrected empirically for absorption effects using ψ scans for 6 reflections having 2θ between 6° and 27° (the relative transmission factors ranged from 0.45 to 1.00), before reducing them to relative squared amplitudes, $|F_o|^2$, by means of standard Lorentz and polarization corrections.

Of the 6256 reflections examined, 1561 were eventually rejected as objectively unobserved by applying the rejection criterion, $I < 3.0\sigma(I)$ were $\sigma(I)$ is the standard deviation in the intensity computed from

$$\sigma^2(I) = (C_t + k^2B)$$

C_t being the total count from scanning, k the ratio of scanning time to background time (in this case $k = 2$), and B the total background count.

All 6256 independent reflections were used to calculate a Wilson plot and were then reduced to a corresponding set of normalized structure factors, E_{hkl}. The values of the various statistical indicators using these normalized structure factors indicated a centrosymmetric space group. Those 172 reflections having the largest E values were then used in the centrosymmetric space group $P\bar{1}$ to locate the metal atom framework of the anion by direct methods (MULTAN). The E map calculated by using a trial set of statistical phases contained five independent peaks which were significantly above the remaining ones and were presumed to be the metal atom sites of the anion. These five atoms were oriented about the crystallographic inversion center at the origin of the unit cell and described half of the metal framework for a $M_{10}O_{28}^{n-}$ polyoxo anion.[20] The fractional coordinates, isotropic thermal parameters and occupancy factors of these five metal atoms were refined as W atoms with use of unit-weighted full-matrix least-squares techniques; these refinement cycles resulted in a conventional unweighted residual,[21] $R_1 = 0.185$, and a conventional weighted residual,[21] $R_2 = 0.220$, for 2832 independent reflections having $2\theta_{\text{Mo K}\bar{\alpha}} < 42.9°$ and $I > 3\sigma(I)$. The five metal occupancy factors refined to values of 1.00 (–), 0.59 (1), 0.37 (1), 0.27 (1), and 0.25 (1), respectively. A difference Fourier calculated at this point contained peaks which appeared to be the 14 oxygen atoms for half of a $M_{10}O_{28}^{n-}$ polyoxo anion[20] and cationic non-hydrogen atoms. Inclusion of these atoms in the isotropic least-squares refinement gave $R_1 = 0.147$ and $R_2 = 0.158$ for 2832 reflections; incorporation of anisotropic thermal parameters for the six metals gave $R_1 = 0.137$ and $R_2 = 0.151$ for 2832 reflections. The resulting $M_{10}O_{28}^{n-}$ anion is shown in Figure 2. Although such a species would belong to a known polyoxoanionic structural class,[20] its presence in crystals of **1** was not consistent with the available analytical or spectroscopic data that indicated the presence of a noncentrosymmetric $\{[(CH_3)_5C_5]Rh(Nb_2W_4O_{19})\}^{2-}$ anion.

Statistical "direct methods" phasing was therefore pursued for **1** in (the noncentrosymmetric) space group $P1$. The resulting E map contained 7 peaks that were significantly higher than the others and located at the vertices of a C_{3v} monocapped octahedron with edge lengths of ~3.3 Å. Unit-weighted full-matrix least-squares refinement cycles which treated the six peaks describing an octahedron as isotropic W atoms and the seventh, capping peak as an isotropic Rh atom gave $R_1 = 0.142$ and $R_2 = 0.183$ for 2832 independent absorption-corrected reflections having $2\theta_{\text{Mo K}\bar{\alpha}} < 42.9°$ and $I > 3\sigma(I)$. The remaining 63 independent non-hydrogen atoms of the asymmetric unit for **1** (Figures 3 and 4[17]) were located by using standard difference Fourier techniques. Their inclusion into the isotropic model for unit-weighted least-squares refinement gave $R_1 = 0.068$ for 2832 reflections. Additional isotropic refinement cycles included variable occupancies for the six metals assigned W scattering factors and resulted in essentially equal (0.97–1.03) occupancies and isotropic thermal parameters (6.0–7.1 Å^2) for all of them. These six

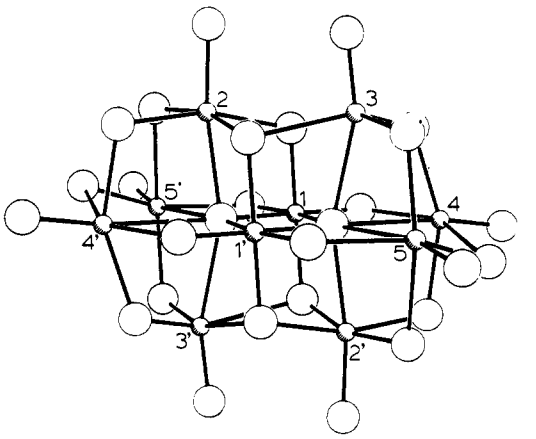

Figure 2. Perspective ORTEP plot of the $M_{10}O_{28}^{n-}$ anion which resulted from the structure solution attempted for **1** in the centrosymmetic triclinic space group $P_{\bar{1}}$. Metal atoms are labeled with numbers and are represented by thermal vibration ellipsoids drawn to encompass 50% of the electron density. Oxygen atoms are not labeled. Metal atoms labeled with a prime (′) are related to those labeled without a prime by the crystallographic inversion center at the origin of the unit cell.

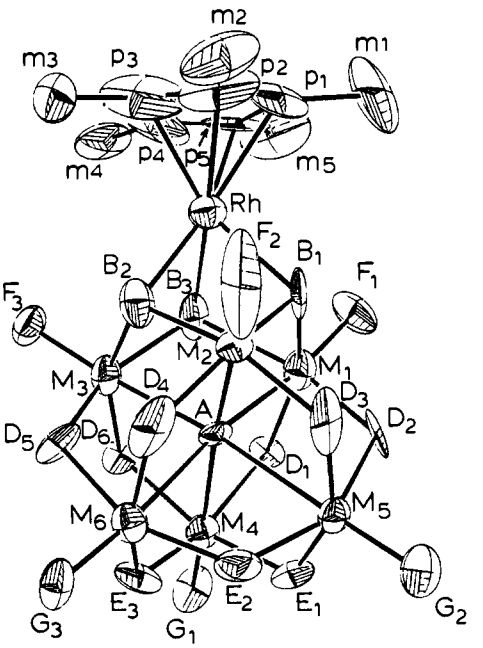

Figure 3. Perspective ORTEP drawing of the non-hydrogen atoms in the solid-state structure for the $\{[\eta^5\text{-}(CH_3)_5C_5]Rh(cis\text{-}Nb_2W_4O_{19})\}^{2-}$ anion. All atoms are represented by thermal vibration ellipsoids drawn to encompass 50% of the electron density. The six disordered niobium/tungsten atom sites in the anion are labeled as M_1–M_6 and the rhodium as Rh. $(CH_3)_5C_5^-$ ligand ring and methyl carbon atoms are labeled by their subscripts p_1–p_5 and m_1–m_5, respectively. Oxygen atoms are labeled by their subscripts according to the following scheme: O_A is the unique six-coordinate oxygen; O_{B_1}–O_{B_3}, O_{D_1}–O_{D_6}, and O_{E_1}–O_{E_3} are doubly bridging oxygens; O_{F_1}–O_{F_3} and O_{G_1}–O_{G_3} are terminally bound oxygens. In the text, metal atoms M_1, M_2, and M_3 are collectively designated M_u atoms while M_4, M_5, and M_6 are designated M_d atoms.

(20) Cotton, F. A.; Wilkinson, G. "Advanced Inorganic Chemistry"; 4th ed.; Wiley: New York, 1980; p 713.

(21) The R values are defined as $R_1 = \sum||F_o| - |F_c||/\sum|F_o|$ and $R_2 = \{\sum w(|F_o| - |F_c|)^2/\sum w|F_o|^2\}^{1/2}$, where w is the weight given each reflection. The function minimized is $\sum w(|F_o| - K|F_c|)^2$, where K is the scale factor.

Table II. Fractional Atomic Coordinates for Non-Hydrogen Atoms in Crystalline $\{[(CH_3)_5C_5]Rh(cis\text{-}Nb_2W_4O_{19})\}[(n\text{-}C_4H_9)_4N]_2$ (1)[a]

atom type[b]	10^3x	10^3y	10^3z	atom type[b]	10^3x	10^3y	10^3z
	Anion				Cation 1		
M_1[c]	159.9 (1)	2.7 (1)	174.9 (1)	N	133 (2)	690 (2)	711 (2)
M_2[c]	247.4 (1)	−139.2 (1)	363.7 (1)	C_{a1}	51 (3)	825 (2)	788 (3)
M_3[c]	181.4 (1)	180.2 (1)	474.2 (1)	C_{a2}	64 (3)	600 (2)	599 (2)
M_4[c]	−88.9 (1)	139.9 (1)	314.6 (1)	C_{a3}	180 (3)	619 (2)	784 (2)
M_5	−22.3 (1)	−174.5 (1)	205.6 (1)	C_{a4}	253 (4)	721 (3)	675 (3)
M_6[c,d]	0.0 (−)[d]	0.0 (−)[d]	500.0 (−)[d]	C_{b1}	−58 (4)	787 (4)	827 (3)
Rh	424.3 (2)	29.8 (2)	335.0 (2)	C_{b2}	5 (2)	660 (2)	510 (2)
O_A	93 (2)	6 (2)	341 (2)	C_{b3}	269 (2)	679 (3)	897 (2)
O_{B1}	298 (2)	−107 (2)	228 (1)	C_{b4}	341 (4)	613 (4)	604 (5)
O_{B2}	306 (2)	36 (1)	465 (1)	C_{g1}	−127 (4)	933 (4)	884 (4)
O_{B3}	250 (2)	149 (1)	317 (1)	C_{g2}	−82 (3)	568 (3)	413 (2)
O_{D1}	13 (1)	119 (1)	191 (1)	C_{g3}	303 (5)	588 (5)	966 (4)
O_{D2}	70 (2)	−145 (2)	100 (1)	C_{g4}	457 (5)	680 (5)	626 (8)
O_{D3}	136 (2)	−247 (1)	253 (1)	C_{d1}	−239 (7)	918 (6)	889 (6)
O_{D4}	154 (2)	−100 (2)	494 (2)	C_{d2}	−186 (3)	545 (3)	445 (3)
O_{D5}	105 (1)	136 (1)	575 (1)	C_{d3}	386 (5)	483 (6)	891 (5)
O_{D6}	32 (1)	257 (1)	425 (1)	C_{d4}	547 (9)	617 (9)	565 (7)
O_{E1}	−142 (1)	−25 (2)	214 (1)		Cation 2		
O_{E2}	−64 (2)	−131 (2)	364 (2)	N	13 (2)	319 (2)	−26 (2)
O_{E3}	−119 (1)	112 (1)	448 (2)	C_{a1}	−77 (3)	269 (3)	2 (3)
O_{F1}	230 (2)	4 (2)	56 (2)	C_{a2}	−21 (2)	404 (2)	−101 (2)
O_{F2}	344 (4)	−203 (3)	378 (2)	C_{a3}	93 (3)	412 (3)	93 (3)
O_{F3}	258 (2)	315 (2)	570 (1)	C_{a4}	96 (2)	205 (2)	−96 (2)
O_{G1}	−209 (1)	240 (1)	297 (1)	C_{b1}	−176 (3)	385 (4)	68 (2)
O_{G2}	−97 (2)	−299 (1)	111 (2)	C_{b2}	−101 (4)	332 (3)	−215 (2)
O_{G3}	−54 (2)	2 (1)	622 (1)	C_{b3}	157 (4)	333 (4)	163 (3)
C_{p1}	585 (2)	−67 (2)	239 (3)	C_{b4}	223 (3)	215 (3)	−127 (2)
C_{p2}	610 (3)	−59 (6)	346 (3)	C_{g1}	687 (7)	361 (9)	89 (8)
C_{p3}	606 (3)	53 (8)	439 (4)	C_{g2}	−145 (3)	415 (3)	−273 (2)
C_{p4}	562 (4)	150 (7)	385 (5)	C_{g3}	220 (3)	441 (3)	284 (3)
C_{p5}	550 (2)	71 (3)	259 (4)	C_{g4}	294 (5)	91 (3)	−185 (3)
C_{m1}	584 (7)	−169 (5)	103 (6)	C_{d1}	630 (6)	286 (7)	980 (8)
C_{m2}	657 (4)	−164 (4)	389 (5)	C_{d2}	−247 (4)	520 (3)	−217 (4)
C_{m3}	614 (3)	137 (4)	568 (3)	C_{d3}	340 (6)	443 (7)	228 (5)
C_{m4}	533 (3)	301 (3)	430 (4)	C_{d4}	421 (5)	93 (7)	−234 (5)
C_{m5}	525 (4)	125 (6)	154 (4)				

[a] Numbers in parentheses are the estimated standard deviations in the last significant digit. [b] Atoms are labeled in agreement with Figures 3 and 4. [c] The disordered polyoxoanionic metal atoms are labeled M_1–M_6 and have 33% Nb character and 67% W character. [d] This atom was used to fix the unit cell origin; its coordinates are therefore listed without estimated standard deviations.

lattice positions therefore appeared to be equivalent with each presumably having $^1/_3$ Nb and $^2/_3$ W character as a result of a statistical disordering of the 2 Nb and 4 W atoms in each anion among them. All subsequent structure factor calculations employed occupancies of 1.00 for these atoms and scattering factors and anomalous dispersion corrections which were 33-$^1/_3$% Nb and 66-$^2/_3$% W in character.

Unit-weighted refinement with anisotropic thermal parameters for all metal atoms, isotropic thermal parameters for all O, N, and C atoms, and mixed form factors and unit occupancies for the disordered metal sites gave $R_1 = 0.049$ and $R_2 = 0.054$ for the 2832 reflections having $2\theta_{Mo\ K\alpha} < 42.9°$ and $I > 3\sigma(I)$. Incorporation of anisotropic thermal parameters for all 70 nonhydrogen atoms with the more complete ($2\theta_{Mo\ K\alpha} < 54.9°$) data set for additional cycles of unit-weighted full-matrix least-squares refinement gave $R_1 = 0.050$ and $R_2 = 0.054$ for 4695 reflections having $I > 3\sigma(I)$. As a further check on the nature of the anion disorder, the site occupancy factors for the six disordered atoms were then alllowed to vary in additional cycles of anisotropic unit-weighted refinement; since none refined to values significantly different from unity, they were fixed at values of 1.00 in the final cycles.

The final cycles of empirically weighted[22] full-matrix least-squares refinement that utilized anisotropic thermal parameters for all 70 nonhydrogen atoms (Table II and III[17]) gave $R_1 = 0.049$ and $R_2 = 0.062$ for 4695 independent reflections having $2\theta_{Mo\ K\alpha} < 54.9°$ and $I > 3\sigma(I)$. During the final cycle of refinement, no parameter shifted by more than 0.32 σ_p with the average shift being less than 0.05 σ_p, where σ_p is the estimated standard deviation for the individual parameter in question. Since a careful comparison of final $|F_o|$ and $|F_c|$ values[17] indicated the absence of extinction effects, extinction corrections were not made.

The correctness of the enantiomeric description for **1** was checked by inverting the coordinates for all 70 anisotropic nonhydrogen atoms and refining them by unit-weighted full-matrix least squares; these cycles converged to $R_1 = 0.051$ and $R_2 = 0.055$ for 4695 reflections.

All structure factor calculations employed recent tabulations of atomic form factors[18b] and anomalous dispersion corrections[18c] to the scattering factors of the W, Nb, and Rh atoms. All calculations were performed on a Data General Eclipse S-200 computer equipped with 64K of 16-bit words, a floating point processor for 32- and 64-bit arithmetic, and versions of the EXTL interactive crystallographic software package as modified at Crystalytics Company.

Results

Synthesis and ^{1}H NMR Measurements. Treatment of $(cis\text{-}Nb_2W_4O_{19})[(n\text{-}C_4H_9)_4N]_4$ with $\{[(CH_3)_5C_5]RhCl_2\}_2$ in CH_2Cl_2 at ambient temperature according to eq 1 results in the formation of an air-stable precipitate which after recrystallization from

$$(Nb_2W_4O_{19})^{4-} + \{[(CH_3)_5C_5]RhCl_2\}_2 \xrightarrow{CH_2Cl_2} \{[(CH_3)_5C_5]Rh(Nb_2W_4O_{19})\}^{2-} + 2Cl^- \quad (1)$$

CH_3CN analyzes as $\{[(CH_3)_5C_5]Rh(Nb_2W_4O_{19})\}[(n\text{-}C_4H_9)_4N]_2$ (**1**). The progress of the reaction can be monitored at low temperature by ^{1}H NMR spectroscopy in the $(CH_3)_5C_5$ region: as

(22) Empirical weights were calculated from the equation $\sigma = \sum_0^3 a_n|F_o|^n = 2.37 - (1.11 \times 10^{-2})|F_o| + (2.29 \times 10^{-4})|F_o|^2 - (3.61 \times 10^{-7})|F_o|^3$, the a_n being coefficients derived from the least-squares fitting of the curve: $||F_o| - |F_c|| = \sum_0^3 a_n|F_o|^n$, where F_c values were calculated from the fully refined anisotropic model using unit weighting and mixed from factors and unit occupancies for the disordered metals.

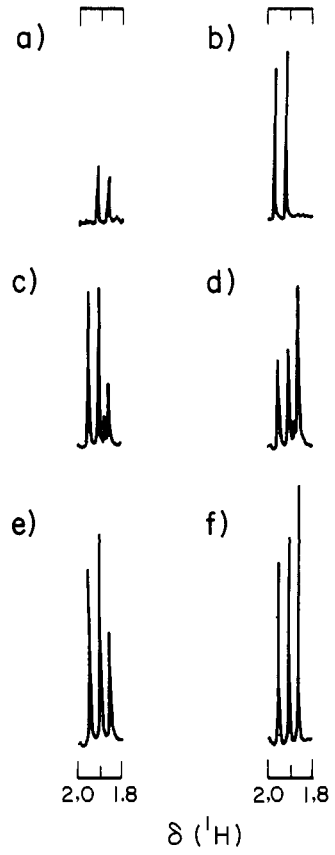

Figure 5. ^1H NMR spectra (360 MHz) of $\{[(CH_3)_5C_5]Rh(Nb_2W_4O_{19})\}[(n\text{-}C_4H_9)_4N]_2$ (**1**) in the δ 1.8–2.0 region: (a) CD_2Cl_2 solution, 0.40 mM in $\{[(CH_3)_5C_5]RhCl_2\}_2$ and 0.80 mM in $(Nb_2W_4O_{19})[(n\text{-}C_4H_9)_4N]_4$, after 0.5 h at −20 °C; (b) same solution as in a at 25 °C; (c) saturated CD_3NO_2 solution of **1**, prepared according to eq 1, ca. 0.5 h after addition of $\{[(CH_3)_5C_5]Rh(NCCH_3)_3\}(PF_6)_2$; (d) same solution as in c at equilibrium; (e) saturated CD_3NO_2 solution of **1** prepared according to eq 1 after being heated for 5 h at 75 °C; and (f) saturated CD_3NO_2 solution of **1** prepared according to eq 1 after equilibrium has been reached with heating (75 °C) for 26 h. The spectrum in a was measured at −20 °C, and the remaining spectra were measured at ambient temperature. The low-intensity 1.88-ppm resonances in c and d are due to the $(CH_3)_5C_5$ protons of $\{[(CH_3)_5C_5]Rh(NCCH_3)_3\}(PF_6)_2$.

the $\{[(CH_3)_5C_5]RhCl_2\}_2$ resonance disappears, two new resonances appear in the δ 1.8–2.0 region at approximately equal rates as shown in Figure 5a. After being warmed to 25 °C, the reaction solution still displays two $(CH_3)_5C_5$ resonances having approximately equal intensities (see Figure 5b). The same spectrum is obtained 24 h after dissolving the compound into CD_3NO_2 at ambient temperature, but addition of $\{[(CH_3)_5]Rh(NCCH_3)_3\}(PF_6)_2$ in relatively small amounts caused a third $[(CH_3)_5C_5]$ resonance to appear within 30 min (see Figure 5c). At equilibrium, the spectrum shown as Figure 5d is obtained. This transformation can also be effected at elevated temperature in the absence of solvated $[(CH_3)_5C_5]Rh^{2+}$. The spectrum shown in Figure 5e was measured after 5 h at 75 °C in CD_3NO_2; the spectrum shown in Figure 5f was measured after the system reached equilibrium (ca. 24 h at 75 °C in CD_3NO_2). Compound **1** also displays the spectrum shown in Figure 5f when prepared according to the reaction

$$(Nb_2W_4O_{19})^{4-} + \{[(CH_3)_5C_5]Rh(NCCH_3)_3\}^{2+} \xrightarrow{CH_3CN/CH_2Cl_2} \{[(CH_3)_5C_5]Rh(Nb_2W_4O_{19})\}^{2-} + 3CH_3CN \quad (2)$$

Solid-State Structure of $\{[(CH_3)_5C_5]Rh(cis\text{-}Nb_2W_4O_{19})\}[(n\text{-}C_4H_9)_4N]_2$. X-ray structural analysis revealed that single crystals of **1**, prepared as a three-diastereomer mixture, are composed of discrete, disordered $\{[(CH_3)_5C_5]Rh(Nb_2W_4O_{19})\}^{2-}$ anions (Figure 3) and $N(n\text{-}C_4H_9)_4^+$ cations (Figure 4).[17] Final atomic coordinates and anisotropic thermal parameters for non-hydrogen atoms of **1** are given with estimated standard deviations in Tables II and III,[17] respectively. Bond lengths and angles for the $\{[(CH_3)_5C_5]Rh(Nb_2W_4O_{19})\}^{2-}$ anion and two $N(n\text{-}C_4H_9)_4^+$ cations are given in Tables IV and V,[17] respectively.

Given the disordered anion structure shown in Figure 3 and the cis stereochemistry for niobiums in the C_{2v} $Nb_2W_4O_{19}^{4-}$ structure f,[23] three diastereomeric structures I–III shown in Figure 6a–c are possible for the anion of **1**. The crystallographic

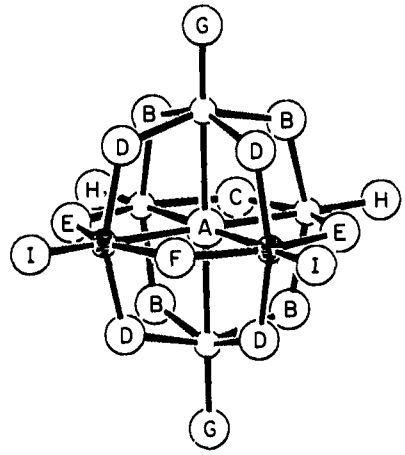

f

equivalence of all six $Nb_2W_4O_{19}^{4-}$ metal atoms precludes the exclusive presence of diastereomer I or III, but it can be accounted for by cocrystallization of either (1) racemic diastereomer II, (2) equal amounts of I and III, or (3) a combination of I and 2. Each of the three possibilities could produce six equivalent $Nb_2W_4O_{19}^{4-}$ metal atom sites with the observed $33^1/_3$% Nb and $66^2/_3$% W character, but only possibility 3 is consistent with the ^1H NMR spectroscopic data presented above.

^{17}O NMR Measurements. According to the ^1H NMR and X-ray crystallographic results just described, all three diastereomers of the $\{[(CH_3)_5C_5]Rh(Nb_2W_4O_{19})\}^{2-}$ anion shown in Figure 6a–c are present at equilibrium. Only two of these are formed, however, when **1** is prepared according to reaction 1. An ^{17}O NMR study was performed to determine which two isomers are formed.

Compound **1** has low solubility in low viscosity solvents like CH_3CN that are suitable for ^{17}O NMR measurements and must be enriched in ^{17}O before ^{17}O NMR measurements can be made. Since enrichment of compound **1** by oxygen exchange with enriched water would almost certainly be complicated by selective exchange effects (see below), enriched **1** was prepared from enriched $(Nb_2W_4O_{19})[(n\text{-}C_4H_9)_4N]_4$. This compound completely exchanges its ONb and ONb_2 oxygens (O_F and O_I in f) with enriched water in CH_3CN in less than 10 min at 25 °C and its ONbW oxygens (O_D and O_E in f) within 24 h according to ^{17}O spectroscopy. Attempts to significantly enrich both OW (O_G and O_H in f) and OW_2 (O_B and O_C in f) oxygens in this fashion unfortunately fail in a practical sense even at elevated temperatures due to sample decomposition. Heating a slurry of $(Nb_2W_4O_{19})[(n\text{-}C_4H_9)_4N]_4$ in $(n\text{-}C_4H_9)_4NOH/H_2O$, however, does significantly exchange all types of oxygens but the central ONb_2W_4 oxygen in the $Nb_2W_4O_{19}^{4-}$ anion. Here, "significantly" means greater than about 75% since the extent of exchange is estimated by ^{17}O NMR spectroscopy.

Oxygen-17 NMR spectra of the two- and three-diastereomer mixtures of **1** are shown in Figures 6 and 7. Chemical shift data are tabulated in Table I. In Figure 6 and Table I, resonances are assigned to specific chemical environments defined by the number

(23) The *cis* assignment is supported by IR data analyzed in ref 3, electrochemical measurements reported in ref 4, ^{17}O NMR spectra described in ref 5 and this paper, and ^{183}W NMR data also reported in this paper.

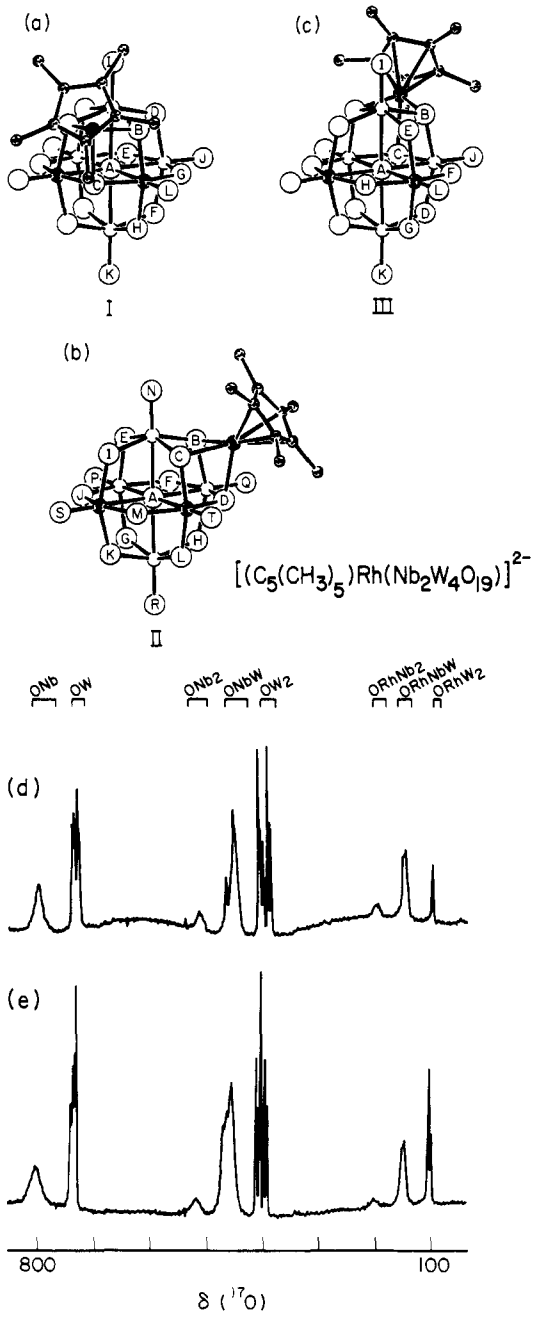

Figure 6. SCHAKAL drawings of the three diastereomers of the $\{[(CH_3)_5C_5]Rh(Nb_2W_4O_{19})\}^{2-}$ anion are shown in a–c. Within the $Nb_2W_4O_{19}$ portion of each anion, the shaded circles represent niobium atoms, the small open circles represent tungsten atoms, and the large open circles represent oxygen atoms. One member of each set of symmetry-equivalent oxygen atoms is labeled. Within the $[(CH_3)_5C_5]Rh$ portion of each anion, shaded circles represent carbons or methyl groups and the filled circles represent the rhodium atom. Assuming rapid rotation of the $[(CH_3)_5C_5]$ ligand, diastereomer I and C_s symmetry, diastereomer II has C_1 symmetry, and diastereomer III has C_s symmetry. ^{17}O NMR spectra (33.9 MHz) of **1** as a two-diastereomer mixture in CH_3CN at 27 °C and of **1** as a three-diastereomer mixture in CH_3CN at 79 °C are shown in d and e, respectively. See Table I for numerical data and the Experimental Section for spectral parameters. Expansions of the OW and OW_2 regions are displayed in Figure 7.

and identities of metals to which each type of oxygen is bonded. These assignments are made by reference to chemical shifts for oxygens having similar environments in simpler molecules.[5,11,24] Note that resonances for all oxygens bonded to niobium are severely broadened by spin–spin coupling to quadrupolar, spin $^9/_2$, 100% abundant ^{93}Nb nuclei.

Examination of the ^{17}O NMR spectrum (see Figure 6d) of the two-diastereomer mixture in the $ORhNb_2$ and OW_2 regions reveals

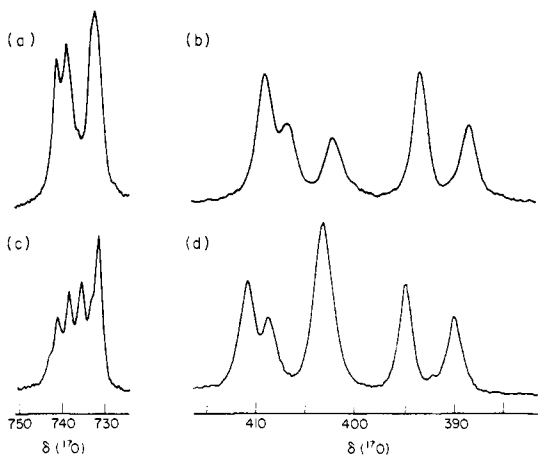

Figure 7. Expansions of the δ 730–750 and 385–415 regions of the ^{17}O NMR spectrum of compound **1** as a two-diastereomer mixture shown in Figure 6d are given in a and b. Parts c and d give expansions of the same regions of the ^{17}O NMR spectrum of **1** as a three-diastereomer mixture shown in Figure 6e.

the identities of the two isomers present. Of all three possible isomers, only isomer I contains an $ORhNb_2$ oxygen (O_C in Figure 6a). Since the spectrum in question displays an $ORhNb_2$ resonance, the two-diastereomer mixture must contain isomer I. In the OW_2 region shown in Figure 7b, five resonances are observed. Isomer I has three types of OW_2 oxygens (O_D, O_E, and O_F in Figure 6a), isomer II has four types of OW_2 oxygens (O_E, O_F, O_G, and O_H in Figure 6b), and isomer III has only one type of OW_2 oxygen (O_D in Figure 6c). The observation of five resonances therefore identifies the second diastereomer as isomer II, since the presence of isomers I plus II implies up to seven OW_2 resonances whereas isomers I plus III can yield at most four. All other features of the ^{17}O NMR spectrum of the two-diastereomer mixture are consistent with the presence of isomers I and II.

The attentive reader may have noticed that the observed intensities in the OW_2 region of the spectrum of the two-isomer mixture (Figure 7b) approximate a 2:1:1:2:1 pattern and that such a pattern cannot result from an equimolar mixture of diastereomers I and II if all OW_2 oxygen sites are enriched in ^{17}O to the same extent. This observation can be explained by assuming that the OW_2 oxygens in the $Nb_2W_4O_{19}^{4-}$ starting material were not enriched statistically but preferentially at the four O_B oxygens sites (see f) with very little enrichment occurring at the unique OW_2 oxygen site, O_C in f. This assumption also explains (a) the intensity pattern for the major resonances in the OW_2 region of the spectrum of the three-diastereomer mixture (Figure 7d), which approximates 2:1:3:2:1; (b) the presence of a very low intensity resonance at 392 ppm in the OW_2 region of the spectrum of the three-diastereomer mixture, which could arise from either of the two oxygens originating in $Nb_2W_4O_{19}^{4-}$ at the low-enrichment site O_C in f, namely, O_E in isomer I or O_F in isomer II, and (3) the approximate 2:1 intensity ratio for the $ORhW_2$ resonances in the spectrum of the three-diastereomer mixture which should be 3:1 (or 1:1) if all $ORhW_2$ sites are equally enriched in ^{17}O. This selective enrichment problem clearly deserves closer examination. Note, however, that it has no bearing on the identification of isomers I and II in the two-diastereomer mixture, since the identification is based solely upon numbers of resonances without regard to their relative intensities.

Discussion

Structure and Stability. The gross structure of the $\{[(CH_3)_5C_5]Rh(Nb_2W_4O_{19})\}^{2-}$ anion combines well-known features of related inorganic and organometallic species. As shown in Figure 3, the Rh^{III} atom achieves an 18-electron configuration by binding to a $[\eta^5\text{-}(CH_3)_5C_5]^-$ ligand and three contiguous bridging oxygen atoms of a disordered $Nb_2W_4O_{19}^{4-}$ anion. This mode of $M_6O_{19}^{n-}$ binding has been observed previously for $Nb_6O_{19}^{8-}$ in $[Mn(Nb_6O_{19})_2]^{12-}$;[25] $Nb_2W_4O_{19}^{4-}$ in $[(OC)_3M$-

$(Nb_2W_4O_{19})]^{3-}$, M = Mn and Re;[5] and $[(C_5H_5)Ti(Mo_5O_{18})]^{3-}$ in its $Mn(CO)_3^+$ and MoO_2Cl^+ adducts.[26] The average Rh–C distance of 2.13 (4, 6, 11, 5) Å[27] is typical for a $[\eta^5\text{-}(CH_3)_5C_5]Rh^{III}$ unit bount to three oxygens: the related species, $\{[(CH_3)_5C_5]Rh(\eta^1\text{-}NO_3)(\eta^2\text{-}NO_3)\}$ (**2**)[28] and $\{[(CH_3)_5C_5]_2Rh_2(\mu\text{-}OH)_3\}^+$ (**3**),[29] have average Rh–C distances of 2.127 (4, 6, 10, 5) and 2.127 (5, 3, 8, 6) Å, respectively. The 2.20 (2, 4, 6, 3) Å average Rh–O bond length in **1** is comparable to the 2.186 (4, 2, 2, 2)-Å Rh-to-bidentate NO_3 Rh–O bond length in **2**.[28] It is longer than the 2.135 (4)-Å Rh-to-monodentate NO_3 Rh–O bond in **2**[28] and the 2.112 (4, 7, 12, 4)-Å average Rh–O bond in **3**.[29] Structural parameters within the pentamethylcyclopentadienyl ring and the tetra-*n*-butylammonium cations are unexceptional when the imprecision of the structure determination is taken into account.

The compatibility of the polyoxohexametallate and pentamethylcyclopentadienyl ligands evident from the space-filling drawing g[6] is remarkable. There are a number of nonbonded interactions at, or slightly longer than, the van der Waals contact

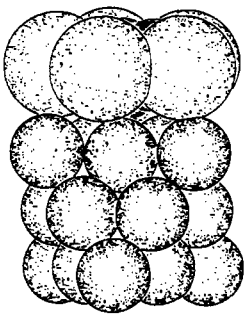

g

distances involving the five ring-carbon atoms and their methyl groups with the six oxygen atoms of the hexametallate surface. These contacts arise in part from the similar dimensions of the two ligands. The largest circle that can be drawn tangential to van der Waals spheres for the peripheral oxygens on the polyoxohexametallate surface (see h[6]) has a 4.7-Å radius, and the analogous circle drawn to encompasss van der Waals spheres for the methyl groups in the $[(CH_3)_5C_5]$ ligand (see i[6]) also has a 4.7-Å radius.

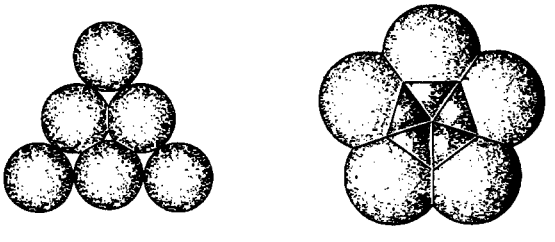

h i

The overall stability of the $\{[(CH_3)_5C_5]Rh(cis\text{-}Nb_2W_4O_{19})\}^{2-}$ ion is not surprising in light of the structural features just outlined, but the approximate 1:1:1 equilibrium distribution of its three diastereomers (see Figures 6a–c) is difficult to rationalize from

Scheme I

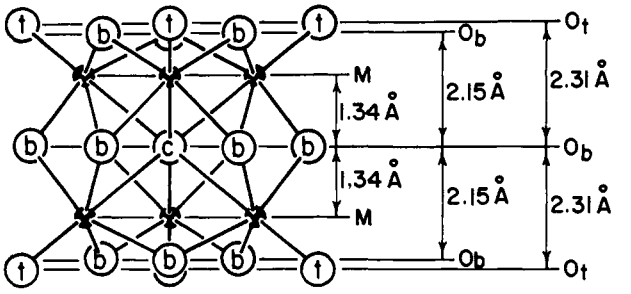

Scheme II

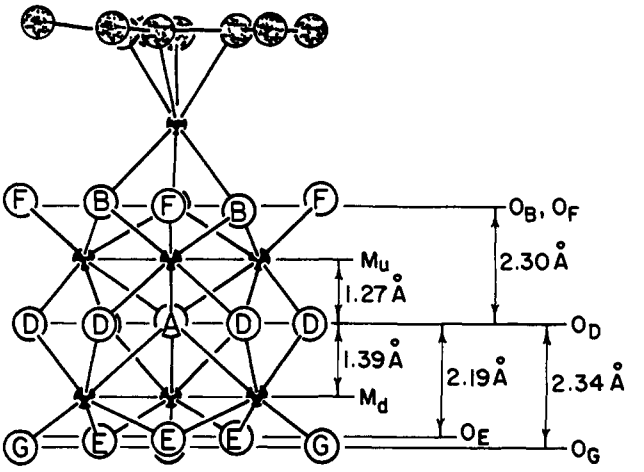

either an entropic or enthalpic point of view. Purely statistical considerations based on symmetry alone yield a I:II:III ratio of 1:2:1 at equilibrium. The observed 1:1:1 distribution therefore indicates that diastereomer II is energetically disfavored relative to I and III. Since this situation differs from that observed for the $[(OC)_3M(Nb_2W_4O_{19})]^{3-}$ M = Mn and Re cases,[5,10] the factors controlling binding site preferencs are unclear. More important, however, these observations clearly indicate that reactive bridging oxygens in the *cis*-$Nb_2W_4O_{19}^{4-}$ ion are not localized about the Nb^V centers. Instead, surface charge can be very effectively delocalized over the surface of the anion, extending to those bridging oxygens bonded only to W^{VI} centers.

Since the crystal structure of **1** displays $Nb_2W_4O_{19}^{4-}$ disorder, a detailed structural picture cannot be provided for the effect of Rh^{III} bonding on the anion framework. Nonetheless, a crude but statistically significant picture of the structural perturbations resulting from cation binding can be obtained from the average structural parameters given in Table IV. Binding of Rh^{III} to the bridging oxygens in $Nb_2W_4O_{19}^{4-}$ causes a lengthening of M_u–O_B bonds (see Table IV and Figure 3) and establishes a pattern of trans bond length alternation[30] evident from the sequence of bond distances $d_{M_u-O_B}$ = 2.05 (2, 3, 7, 6) Å,[27] $d_{M_u-O_D}$ = 1.91 (2, 2, 5, 6) Å, $d_{M_d-O_D}$ = 1.95 (2, 2, 5, 6) Å, and $d_{M_d-O_E}$ = 1.92 (2, 3, 8, 6) Å.[30] This type of bond length alternation has been observed in the related, ordered $[(C_5H_5)Ti(Mo_5O_{18})MoO_2Cl]^{2-}$ structure,[26] and is also present in the $[Mn(Nb_6O_{19})_2]^{12-}$ structure.[25] Note that bond length alternation provides a mechanism for charge delocalization. The formation of Rh–O_B bonds involves a withdrawal of negative charge from the O_B centers which causes a weakening of M_u–O_B bonds. The resulting strengthening of M_u–O_D bonds causes a proportional withdrawal of electron density from O_D

(24) Klemperer, W. G.; Shum, W. *J. Am. Chem. Soc.* **1978**, *100*, 4891–3.
(25) Flynn, C. M., Jr.; Stucky, G. D. *Inorg. Chem.* **1969**, *8*, 335–44.
(26) Day, V. W.; Fredrich, M. F.; Thompson, M. R.; Klemperer, W. G.; Liu, R.-S.; Shum, W. *J. Am. Chem. Soc.* **1981**, *103*, 3597.
(27) The first number in parentheses following an averaged value of a bond length or angle is the root-mean-square estimated standard deviation of an individual datum. The second and third numbers, when given, are the average and maximum deviations from the averaged value, respectively. The fourth number represents the number of individual measurements which are included in the average value.
(28) Hursthouse, M. B.; Malik, K. M. A.; Mingos, D. M. P.; Willoughby, S. D. *J. Organomet. Chem.* **1980**, *192*, 235–51.
(29) Nutton, A.; Bailey, P. M.; Maitlis, P. M. *J. Chem. Soc., Dalton Trans.* **1981**, 1997–2002.
(30) Many of these bond length differences would be expected to be small and as such perhaps not observable in the present study due to the presence of very "heavy" and disordered W and Nb atoms in a noncentrosymmetric space group with disorder-prone $N(n\text{-}C_4H_9)_4^+$ cations. However, the C_{3v}-averaged structural parameters for the anion of **1** are seen to be totally consistent with a systematic pattern of bond length alternation, and only one bond length pair (M_2–O_{D_4} and M_6–O_{D_4} at 1.91 (2) and 1.90 (2) Å, respectively) is inconsistent.

centers. This in turn causes a weakening of M_d–O_D bonds and strengthening of M_d–O_E bonds, leading to withdrawal of electron density from O_E centers.

The gross effects of Rh^{III} binding on the $Nb_2W_4O_{19}^{4-}$ structure just mentioned can be viewed in a more comprehensive fashion through a comparison of spacings between approximately parallel layers of atoms in the octahedral $W_6O_{19}^{2-}$ anion (Scheme I) with spacings between corresponding layers of atoms in **1** (Scheme II). In the $W_6O_{19}^{2-}$ anion, a set of six bridging O_b oxygen atoms plus the central O_c atom form a convenient reference plane.[31] Three different sets of atoms lie in planes above and below a given reference plane: two equivalent sets of three terminal O_t oxygen atoms, two equivalent sets of three doubly bridging O_b oxygen atoms, and two equivalent sets of three tungsten atoms. These are displaced from this reference plane by 2.314 (7, 21, 45, 24), 2.153 (7, 9, 33, 24), and 1.343 (1, 8, 23, 24) Å, respectively. In **1**, a corresponding reference plane is defined by the six O_D oxygen atoms.[32a] In Scheme II, two sets of atoms are seen to lie above this reference plane in approximately parallel layers: the O_B and O_F atoms are displaced from the reference plane by 2.30 (2, 5, 11, 5) Å[32b] and the M_u atoms by 1.267 (1, 7, 10, 3) Å. The unique central O_A atom lies 0.10 (2) Å above the plane. Three other distinct layers of atoms are displaced below the reference plane, the M_d atoms by 1.393 (1, 8, 12, 3) Å, the O_E atoms by 2.19 (2, 3, 5, 3) Å, and the O_G atoms by 2.34 (2, 1, 2, 3) Å. Comparison of Schemes I and II provides a clear overview of the effect of Rh^{III} binding on the hexametallate structure. Formation of Rh–O_B bonds and weakening of M_u–O_B bonds displaces the O_B centers away from the O_D reference plane such that O_B and O_F centers are approximately coplanar in a configuration quite different from the corresponding O_b and O_t planes in $W_6O_{19}^{2-}$. In contrast, the O_E and O_G layers in Scheme II and their corresponding O_b and O_t layers in Scheme I are separated by about the same distances from their respective reference planes. Both the 1.27 Å M_u and 1.39 Å M_d displacements in **1** differ significantly, however, from the 1.34 Å metal-layer displacements in $W_6O_{19}^{2-}$. Both deviations from the prototypical 1.34-Å value in $W_6O_{19}^{2-}$ are direct consequences of the bond length alternation pattern discussed above.

Diastereomers I and II: Mechanism of Formation. Preparation of compound **1** according to reaction 1 results in formation of $\{[(CH_3)_5C_5]Rh(Nb_2W_4O_{19})\}^{2-}$ exclusively as isomers I and II shown in Figure 6. Since reaction 1 involves both splitting of the $\{[(CH_3)_5C_5]RhCl_2\}_2$ dimer and displacement of two chloride ligands per rhodium, a two-step mechanism is likely:

$$^1/_2\{[(CH_3)_5C_5]RhCl_2\}_2 + Nb_2W_4O_{19}^{4-} \rightarrow \{[(CH_3)_5C_5]RhCl_2(Nb_2W_4O_{19})\}^{4-} \quad (3)$$

$$\{[(CH_3)_5C_5]RhCl_2(Nb_2W_4O_{19})\}^{4-} \rightarrow \{[(CH_3)_5C_5]Rh(Nb_2W_4O_{19})\}^{2-} + 2Cl^- \quad (4)$$

The formation of $[(CH_3)_5C_5]RhCl_2L$, L = $Nb_2W_4O_{19}^{4-}$, is precedented by the formation of L = pyridine, *p*-toluidine, $P(C_6H_5)_3$, and $P(CH_3)_3$ adducts from two-electron donors L and $\{[(CH_3)_5C_5]RhCl_2\}_2$.[13,33] Either terminal or bridging oxygens on the $Nb_2W_4O_{19}^{4-}$ surface may act as two-electron donors, and the proposed intermediate can in principle adopt two different geometries shown in j and m.[34] In the first structure the unidentate

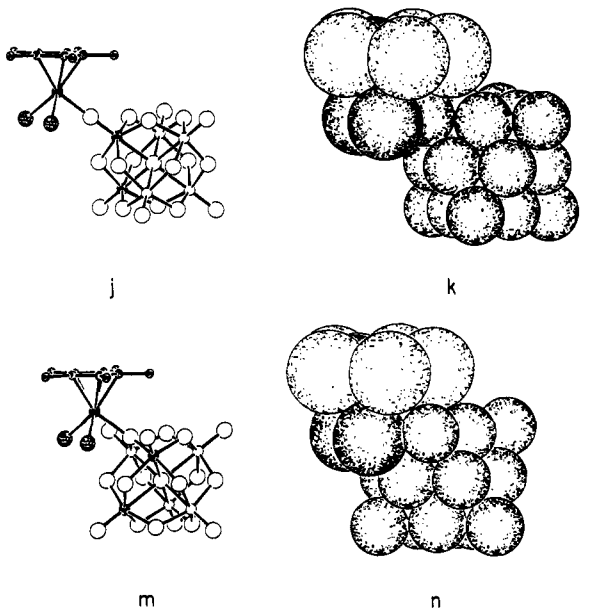

$Nb_2W_4O_{19}^{4-}$ ligand binds to rhodium by using one of its ONb terminal oxygens, O_I in f. This structure places the rhodium center adjacent to the two nonequivalent triangles of oxygen atoms which form rhodium binding sites in isomers I and II (O_D–O_D–O_F and O_B–O_D–O_E in f) but remote from the rhodium binding site in isomer III (O_B–O_B–O_C in f). In the second structure, m, an ONbW oxygen, O_D in f, is bound to rhodium. Diastereomers I and II can be formed from this type of intermediate by breaking two Rh–Cl bonds and forming two Rh–O bonds: no Rh–O bond breaking is involved. All pathways from intermediate m to diastereomer III, however, must involve initial Rh–O bond cleavage.

Although the regiospecificity of reaction 1 can be explained by either intermediate j or m, structure j is a far more likely candidate than m on both steric and electronic grounds. Examination of space-filling representations k and n reveals extreme steric crowding in n resulting from several close oxygen–chlorine contacts. There is precedent for ONb oxygens in *cis*-$Nb_2W_4O_{19}^{4-}$ acting as metal binding sites in the $\{[(C_7H_8)Rh]_5(Nb_2W_4O_{19})_2\}^{3-}$ ion.[35] Furthermore, the structure proposed for this (norbornadiene)rhodium(I) adduct[35] involves binding $(C_7H_8)Rh^+$ units to terminal oxygens only of the ONb type, leaving the sterically equivalent $(C_7H_8)Rh^+$ binding site formed by OW oxygens vacant. This selectivity provides support for the selectivity proposed here for $[(CH_3)_5C_5]RhCl_2$ binding. In a related system, $[(C_5H_5)_3U\text{-}(NbW_5O_{19})_2]^{5-}$, preference for ONb terminal oxygen binding over OW, ONbW, and OW_2 oxygen binding has been observed.[36] Here, the sterically congested $[(C_5H_5)_3U]^+$ unit binds to $NbW_5O_{19}^{3-}$ ligands exclusively at ONb oxygen centers.

Generation of Diastereomer III. The intermolecular mechanism described by reactions 5 and 6, S = CH_3CN or CH_3NO_2, is proposed for the generation of diastereomer III from diastereomers I and II in the presence of solvated $[(CH_3)_5C_5]Rh^{2+}$ since the isomerization proceeds at a very slow rate in the absence of this cation. The intermediates in the proposed mechanism are as-

$$\{[(CH_3)_5C_5]Rh(Nb_2W_4O_{19})\}^{2-} + \{[(CH_3)_5C_5]Rh^*S_3\}^{2+} \rightarrow \underset{\text{diastereomer I and II}}{\{[(CH_3)_5C_5]Rh(Nb_2W_4O_{19})Rh^*[(CH_3)_5C_5]\}} + 3S \quad (5)$$

$$\{[(CH_3)_5C_5]Rh(Nb_2W_4O_{19})Rh^*[(CH_3)_5C_5]\} + 3S \rightarrow \{[(CH_3)_5C_5]RhS_3\}^{2+} + \underset{\text{diastereomer III}}{\{(Nb_2W_4O_{19})Rh^*[(CH_3)_5C_5]\}^{2-}} \quad (6)$$

(31) Eight possibilities exist for such reference planes in the two crystallographically independent and centrosymmetric $W_6O_{19}^{2-}$ anions of the $(n\text{-}C_4H_9)_4N^+$ salt;[7] oxygen atoms in each set are coplanar within 0.011 Å. Distances from this reference plane given in the text and Scheme I are averaged for all eight possibilities.

(32) (a) This reference plane consists of the six O_D atoms in **1**, and the least-squares mean plane through these six atoms, which are coplanar within 0.01 Å, is defined by $0.9548X + 0.1986Y - 0.2212Z = 0.0108$, where X, Y, and Z are orthogonal coordinates measured in angstroms along ($\vec{b} \times \vec{c}^*$), $\vec{b}$, and $\vec{c}^*$, respectively, of the unit cell. (b) The six bridging O_B and terminal O_F oxygens are displaced from the reference plane by an average value of 2.26 (2, 8, 18, 6) Å. If O_{F_2}, whose position is obviously in error because of the unrealistically short 1.24 (4) Å M_2–O_{F_2} bond length, is omitted, this value becomes 2.30 (2, 5, 11, 5) Å.

(33) Isobe, K.; Bailey, P. M.; Maitlis, P. M. *J. Chem. Soc., Dalton Trans.* **1981**, 2003–8.

(34) In j–**n**, 90° Cl–Rh–Cl angles were chosen to match the 91 and 92° Cl–Rh–Cl angles observed at the terminal chlorine ligand in $\{[(CH_3)_5C_5]RhCl_2\}_2$.[8]

(35) Besecker, C. J.; Klemperer, W. G.; Day, V. W. *J. Am. Chem. Soc.* **1982**, *104*, 6158–9.

(36) Day, V. W.; Klemperer, W. G.; Maltbie, D. J., manuscript in preparation.

Table IV. Bond Lengths (Å) and Angles (deg) in the $\{[C_5(CH_3)_5]Rh(cis\text{-}Nb_2W_4O_{19})\}^{2-}$ Anion of **1**[a]

parameter[b]	value	average[c,d]	parameter[b]	value	average[c,d]
		Distances			
M_1-O_{B_1}	2.06 (2)		M_4-O_{E_1}	1.91 (2)	
M_2-O_{B_1}	2.06 (2)		M_5-O_{E_1}	2.00 (2)	
M_2-O_{B_2}	2.04 (2)	M_u-O_B = 2.05 (2, 3, 7, 6)	M_5-O_{E_2}	1.92 (2)	M_d-O_E = 1.92 (2, 3, 8, 6)
M_3-O_{B_2}	1.98 (2)		M_6-O_{E_2}	1.85 (2)	
M_3-O_{B_3}	2.07 (2)		M_6-O_{E_3}	1.95 (2)	
M_1-O_{B_3}	2.10 (2)		M_4-O_{E_3}	1.91 (2)	
M_1-O_{D_1}	1.93 (2)		M_4-O_{D_1}	1.97 (1)	
M_1-O_{D_2}	1.94 (2)		M_5-O_{D_2}	1.95 (2)	
M_2-O_{D_3}	1.86 (2)	M_u-O_D = 1.91 (2, 2, 5, 6)	M_5-O_{D_3}	1.94 (2)	M_d-O_D = 1.95 (2, 2, 5, 6)
M_2-O_{D_4}	1.91 (2)		M_6-O_{D_4}	1.90 (2)	
M_3-O_{D_5}	1.90 (2)		M_6-O_{D_5}	1.94 (2)	
M_3-O_{D_6}	1.90 (2)		M_4-O_{D_6}	1.99 (2)	
M_1-O_A	2.28 (2)		M_4-O_A	2.41 (2)	
M_2-O_A	2.29 (2)	M_u-O_A = 2.27 (2, 2, 2, 3)	M_5-O_A	2.46 (2)	M_d-O_A = 2.43 (2, 2, 3, 3)
M_3-O_A	2.25 (2)		M_6-O_A	2.41 (2)	
M_1-O_{F_1}	1.78 (2)		M_4-O_{G_1}	1.69 (2)	
M_2-O_{F_2}	1.24 (4)	M_u-O_F = 1.59 (3, 24, 35, 3)	M_5-O_{G_2}	1.68 (2)	M_d-O_G = 1.69 (2, 1, 2, 3)
M_3-O_{F_3}	1.76 (2)		M_6-O_{G_3}	1.71 (2)	
Rh-O_{B_1}	2.14 (2)		Rh-C_{p_1}	2.18 (3)	
Rh-O_{B_2}	2.22 (2)	2.20 (2, 4, 6, 3)	Rh-C_{p_2}	2.16 (5)	
Rh-O_{B_3}	2.24 (2)		Rh-C_{p_3}	2.20 (4)	2.13 (4, 6, 11, 5)
			Rh-C_{p_4}	2.08 (6)	
			Rh-C_{p_5}	2.02 (3)	
$M_1\cdots M_2$	3.377 (2)				
$M_1\cdots M_3$	3.373 (2)	M_u-M_u = 3.379 (2, 6, 9, 3)			
$M_2\cdots M_3$	3.388 (2)				
			C_{p_1}-C_{p_2}	1.29 (5)	
$M_4\cdots M_5$	3.327 (2)		C_{p_2}-C_{p_3}	1.32 (8)	
$M_4\cdots M_6$	3.316 (2)	M_d-M_d = 3.320 (2, 4, 7, 3)	C_{p_3}-C_{p_4}	1.54 (12)	1.42 (8, 9, 13, 5)
$M_5\cdots M_6$	3.318 (2)		C_{p_4}-C_{p_5}	1.42 (8)	
			C_{p_1}-C_{p_5}	1.52 (5)	
$M_1\cdots M_4$	3.296 (2)				
$M_1\cdots M_5$	3.302 (2)		C_{p_1}-C_{m_1}	1.59 (8)	
$M_2\cdots M_5$	3.281 (2)		C_{p_2}-C_{m_2}	1.53 (8)	
$M_2\cdots M_6$	3.269 (1)	M_u-M_d = 3.290 (2, 10, 21, 6)	C_{p_3}-C_{m_3}	1.47 (6)	1.57 (8, 6, 10, 5)
$M_3\cdots M_4$	3.296 (2)		C_{p_4}-C_{m_4}	1.61 (9)	
$M_3\cdots M_6$	3.293 (1)		C_{p_5}-C_{m_5}	1.66 (7)	
		Angles, deg			
$M_1O_{B_1}M_2$	110 (1)		$M_4O_{E_1}M_5$	116 (1)	
$M_2O_{B_2}M_3$	115 (1)	111 (1, 3, 4, 3)	$M_5O_{E_2}M_6$	123 (1)	119 (1, 2, 4, 3)
$M_3O_{B_3}M_1$	108 (1)		$M_6O_{E_3}M_4$	119 (1)	
$M_1O_{D_1}M_4$	116 (1)		$M_1O_AM_4$	89 (1)	
$M_1O_{D_2}M_5$	116 (1)		$M_1O_AM_5$	88 (1)	
$M_2O_{D_3}M_5$	119 (1)	117 (1, 1, 2, 6)	$M_2O_AM_5$	87 (1)	89 (1, 1, 2, 6)
$M_2O_{D_4}M_6$	118 (1)		$M_2O_AM_6$	88 (1)	
$M_3O_{D_5}M_6$	118 (1)		$M_3O_AM_6$	90 (1)	
$M_3O_{D_6}M_4$	116 (1)		$M_3O_AM_4$	90 (1)	
$M_1O_AM_2$	95 (1)		$M_4O_AM_5$	86 (1)	
$M_1O_AM_3$	96 (1)	96 (1, 1, 1, 3)	$M_4O_AM_6$	87 (1)	86 (1, 0, 1, 3)
$M_2O_AM_3$	97 (1)		$M_5O_AM_6$	86 (1)	
$M_1O_AM_6$	173 (1)		$RhO_{B_1}M_1$	101 (1)	
$M_2O_AM_4$	172 (1)	173 (1, 1, 1, 3)	$RhO_{B_1}M_2$	98 (1)	
$M_3O_AM_5$	174 (1)		$RhO_{B_2}M_2$	96 (1)	99 (1, 2, 3, 6)
$O_{B_1}RhO_{B_2}$	76 (1)		$RhO_{B_2}M_3$	102 (1)	
$O_{B_1}RhO_{B_3}$	76 (1)	75 (1, 1, 2, 3)	$RhO_{B_3}M_3$	99 (1)	
$O_{B_2}RhO_{B_3}$	73 (1)		$RhO_{B_3}M_1$	97 (1)	
$C_gRhO_{B_1}$[e]	132 (–)		$O_AM_1O_{F_1}$	173 (1)	
$C_gRhO_{B_2}$[e]	135 (–)	135 (–, 2, 2, 3)	$O_AM_2O_{F_2}$	169 (2)	
$C_gRhO_{B_3}$[e]	138 (–)		$O_AM_3O_{F_3}$	176 (1)	174 (1, 2, 5, 6)
			$O_AM_4O_{G_1}$	175 (1)	
$O_{F_1}M_1O_{B_1}$	98 (1)		$O_AM_5O_{G_2}$	178 (1)	
$O_{F_1}M_1O_{B_3}$	98 (1)		$O_AM_6O_{G_3}$	175 (1)	
$O_{F_2}M_2O_{B_1}$	96 (1)	99 (1, 2, 5, 6)			
$O_{F_2}M_2O_{B_2}$	98 (2)		$O_{G_1}M_4O_{E_1}$	104 (1)	
$O_{F_3}M_3O_{B_2}$	104 (1)		$O_{G_1}M_4O_{E_3}$	105 (1)	
$O_{F_3}M_3O_{B_3}$	98 (1)		$O_{G_2}M_5O_{E_1}$	104 (1)	106 (1, 1, 2, 6)
			$O_{G_2}M_5O_{E_2}$	107 (1)	
$O_{F_1}M_1O_{D_1}$	105 (1)		$O_{G_3}M_6O_{E_2}$	108 (1)	
$O_{F_1}M_1O_{D_2}$	105 (1)		$O_{G_3}M_6O_{E_3}$	106 (1)	
$O_{F_2}M_2O_{D_3}$	109 (2)	106 (1, 2, 5, 6)			
$O_{F_2}M_2O_{D_4}$	108 (2)		$O_{G_1}M_4O_{D_6}$	102 (1)	
$O_{F_3}M_3O_{D_5}$	106 (1)		$O_{G_1}M_4O_{D_1}$	102 (1)	
$O_{F_3}M_3O_{D_6}$	101 (1)		$O_{G_2}M_5O_{D_2}$	103 (1)	103 (1, 1, 2, 6)
			$O_{G_2}M_5O_{D_3}$	105 (1)	
			$O_{G_3}M_6O_{D_4}$	102 (1)	
			$O_{G_3}M_6O_{D_5}$	102 (1)	

Table IV (*Continued*)

parameter[b]	value	average[c,d]	parameter[b]	value	average[c,d]
$O_AM_1O_{B3}$	77 (1)	76 (1, 2, 3, 6)	$O_AM_4O_{E3}$	78 (1)	77 (1, 1, 3, 6)
$O_AM_1O_{B1}$	77 (1)		$O_AM_4O_{F1}$	80 (1)	
$O_AM_2O_{B1}$	77 (1)		$O_AM_5O_{E1}$	77 (1)	
$O_AM_2O_{B2}$	73 (1)		$O_AM_5O_{E2}$	74 (1)	
$O_AM_3O_{B2}$	75 (1)		$O_AM_6O_{E2}$	77 (1)	
$O_AM_3O_{B3}$	78 (1)		$O_AM_6O_{E3}$	77 (1)	
$O_AM_1O_{D1}$	79 (1)	79 (1, 1, 1, 6)	$O_AM_4O_{D6}$	74 (1)	75 (1, 1, 1, 6)
$O_AM_1O_{D2}$	80 (1)		$O_AM_4O_{D1}$	75 (1)	
$O_AM_2O_{D3}$	80 (1)		$O_AM_5O_{D2}$	75 (1)	
$O_AM_2O_{D4}$	78 (1)		$O_AM_5O_{D3}$	74 (1)	
$O_AM_3O_{D5}$	78 (1)		$O_AM_6O_{D4}$	75 (1)	
$O_AM_3O_{D6}$	80 (1)		$O_AM_6O_{D5}$	74 (1)	
$O_{B3}M_1O_{B1}$	81 (1)	82 (1, 0, 1, 3)	$O_{E3}M_4O_{E1}$	87 (1)	85 (1, 1, 2, 3)
$O_{B1}M_2O_{B2}$	82 (1)		$O_{E1}M_5O_{E2}$	84 (1)	
$O_{B2}M_3O_{B3}$	82 (1)		$O_{E2}M_6O_{E3}$	85 (1)	
$O_{D1}M_1O_{D2}$	93 (1)	93 (1, 0, 0, 3)	$O_{D6}M_4O_{D1}$	84 (1)	83 (1, 1, 1, 3)
$O_{D3}M_2O_{D4}$	93 (1)		$O_{D2}M_5O_{D3}$	84 (1)	
$O_{D5}M_3O_{D6}$	93 (1)		$O_{D4}M_6O_{D5}$	82 (1)	
$O_{B1}M_1O_{D1}$	156 (1)	154 (1, 1, 2, 6)	$O_{E1}M_4O_{D6}$	154 (1)	152 (1, 1, 2, 6)
$O_{B3}M_2O_{D2}$	156 (1)		$O_{E3}M_4O_{D1}$	153 (1)	
$O_{B2}M_2O_{D3}$	152 (1)		$O_{E2}M_5O_{D2}$	150 (1)	
$O_{B1}M_2O_{D4}$	154 (1)		$O_{E1}M_5O_{D3}$	151 (1)	
$O_{B3}M_3O_{D5}$	155 (1)		$O_{E3}M_6O_{D4}$	152 (1)	
$O_{B2}M_3O_{D6}$	154 (1)		$O_{E2}M_6O_{D5}$	150 (1)	

[a] Numbers in parentheses following an individual value are the estimated standard deviation in the last significant digit. [b] Atoms are labeled in agreement with Tables II and III and Figure 3. The disordered polyoxoanionic metal atoms are labeled M_1-M_6 and have 33% Nb character and 67% W character. [c] See ref 27. [d] Polyoxoanionic metal atoms M_1, M_2, and M_3 are collectively designated as M_u atoms while M_4, M_5, and M_6 are designated as M_d atoms. [e] C_g refers to the center of gravity for the five-carbon ring of the cyclopentadienyl ligand.

sumed to contain reactant anions coordinated to $[(CH_3)_5C_5]$-Rh(III) units using three of their bridging oxygens. Thus reaction 5 involves no metal–oxygen bond breaking, and reaction 6 involves no metal–oxygen bond formation.

Two types of isomerism are possible for the proposed intermediate. The first involves different geometries for the $\{[(CH_3)_5C_5]Rh\}_2(M_6O_{19})$ framework. Since each Rh bound to a triangle of bridging oxygens can be associated with a face of the M_6 octahedron and octahedral faces can be selected pairwise in three different ways, three isomeric frameworks can be envisioned. One isomer, in which the two octahedral faces share an edge, can be ruled out as physically unrealistic since it implies severe $[(CH_3)_5C_5]$ overlap. The other two are physically reasonable. The first, denoted *meta*, involves octahedral faces with a common vertex. The second isomer, denoted *para*, involves nonadjacent faces. Examples of *meta* and *para* isomers are shown in o^6 and p^6, respectively. A second type of isomerism, permutational isomerism, is also possible for each isomer. This is obtained by orienting the Nb_2W_4 octahedron differently within the *meta*- and *para*-$\{[(CH_3)_5C_5]Rh\}_2(cis\text{-}Nb_2W_4O_{19})$ framework. Several distinct isomerization pathways are therefore implied by reactions 5 and 6.

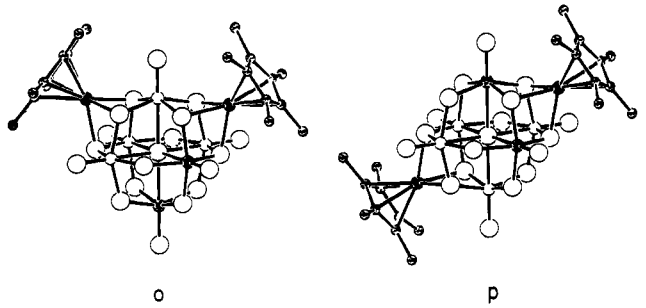

o p

Unresolved Isssues. Three aspects of the above discussion have specific implications that may be subjected to experimental investigation. The first concerns the $\{[(CH_3)_5C_5]RhCl_2(Nb_2W_4O_{19})\}^{4-}$ anion proposed above in reactions 3 and 4. If the proposal is correct, related species $\{[(CH_3)_5C_5]RhX_2(Nb_2W_4O_{19})\}^{4-}$ containing univalent ligands X which are poor leaving groups should be isolable. More generally, adducts of $Nb_2W_4O_{19}^{4-}$ and other sterically congested two-electron acceptors should be stable, and these acceptors should be bound to ONb oxygens. A second family of intermediates, the $\{[(CH_3)_5C_5]Rh\}_2(Nb_2W_4O_{19})$ molecules proposed above in reaction 5, should also be stable, isolable species if the decomposition reaction 6 were blocked by isolation from potential ligands, S. The third unresolved issue implicit in the above discussion is the question of facile interconversion of isomers I and II (see Figure 6). This more subtle question warrants more detailed discussion.

Referring to Figure 5, three striking "coincidences" concerning the relative amounts of isomers I and II are evident, namely, their approximately identical relative concentrations in three different situations: (i) when isomers I and II coexist in CD_2Cl_2 solution at 25 °C in the absence of isomer III (see Figure 5b), (ii) when isomers I, II, and III are at equilibrium in CD_3NO_2 solution at 25 °C (see Figure 5, parts d and f), and (iii) during the course of $[(CH_3)_5C_5]RhS_3^{2+}$-catalyzed generation of isomer III from isomers I and II (see Figure 5c). It is difficult to rationalize this situation without invoking an undetected, "hidden" process that interconverts diasteromers I and II in less than an hour at ambient temperature in either CH_2Cl_2 or CH_3NO_2 solution, i.e., under conditions where isomer III is not generated. Unless such a mechanism is invoked, one must assume that isomer III is generated from isomer I at precisely the same rate it is generated from isomer II, and one must further assume that kinetic control of reaction 1 fortuitously yields an equilibrium mixture of isomers I and II. The former assumption is of course reasonable, but unlikely if the isomerization mechanism proposed in eq 5 and 6 is operative. According to this mechanism, isomer II has access to only one isomer of the $\{[(CH_3)_5C_5]Rh\}_2(Nb_2W_4O_{19})\}$ intermediate, o, which can lead to isomer III. Isomer I, on the other hand, has access to two isomers of the intermediate which can generate isomer III: one *meta* isomer and the *para* isomer p. The possibility that isomers I and II are formed according to reaction 1 at rates not proportional to their equilibrium concentrations might be investigated at low temperature. The ^1H NMR spectrum shown in Figure 5a monitors precisely such a situation in CD_2Cl_2. Taken by itself, the spectrum indicates that isomers I and II are

not necessarily formed at rates proportional to their equilibrium concentrations. Unfortunately, however, the result is inconclusive due to reproducibility problems. These arise from the very low solubility of compound **1** in CD_2Cl_2. The spectra shown in Figure 5, parts a and b, were both measured from supersaturated solutions. Such solutions are exceedingly difficult to deal with on a reproducible basis since spontaneous precipitation occurs on a seemingly random basis. Resolution of this isomerization issue therefore depends upon the development of new experimental approaches.

We note that the existence of a facile process interconverting isomers I and II has significant implications. This process must involve breaking at least two Rh-O bonds and forming at least two new Rh-O bonds. Since the rigidity of the $Nb_2W_4O_{19}^{4-}$ framework precludes a concerted, intramolecular process, the isomerization would have to involve coordinatively unsaturated or solvated rhodium species, possibly of the type j. These species may of course be susceptible to external nucleophilic attack, a possibility currently being investigated.

Acknowledgment. W.G.K. acknowledges the National Science Foundation for partial support of this research. NMR experiments were conducted with assistance from Denny Warrenfeltz at the University of Illinois NSF Regional NMR Facility (Grant CHE97-16100). We are grateful to Dr. Egbert Keller for providing a copy of his SCHAKAL program and to Suzanne M. Moenter for preparing drawings.

Registry No. 1 (isomer I), 90245-26-4; **1** (isomer II), 90245-28-6; **1** (isomer III), 90245-30-0; $(Nb_2W_4O_{19})Na_2[(CH_3)_4N]_2$, 90245-22-0; $(Nb_2W_4O_{19})[(n\text{-}C_4H_9)_4N]_4$, 90245-21-9; $\{[(CH_3)_5C_5]RhCl_2\}_2$, 12354-85-7; $[(CH_3)_5C_5]Rh(NCCH_3)_3^{2+}$, 59738-27-1.

Supplementary Material Available: Crystal structure analysis report, Table III (Anisotropic Thermal Parameters for Nonhydrogen Atoms), Table V (Cation Bond Lengths and Angles), Figure 4 (ORTEP drawings for cations of **1**), and structure factor tables for the X-ray structural study of $\{[(CH_3)_5C_5]Rh(cis\text{-}Nb_2W_4O_{19})\}[(n\text{-}C_4H_9)_4N]_2$ (34 pages). Ordering information can be obtained from any current masthead page.

Influence of Hydrogen Bonding on the Properties of Iron Porphyrin Imidazole Complexes. An Internally Hydrogen Bonded Imidazole Ligand

Robert Quinn,[1a,b] Janet Mercer-Smith,[1b] Judith N. Burstyn,[1b] and Joan Selverstone Valentine*[1a,b]

Contribution from the Department of Chemistry and Biochemistry and Molecular Biology Institute, University of California, Los Angeles, California 90024. *Received November 28, 1983*

Abstract: Two new imidazole derivatives have been synthesized, *cis*-methyl urocanate and *trans*-methyl urocanate. The former has been shown by infrared (IR) spectroscopy to contain an N—H···O=C internal hydrogen bond while the latter self-associates by intermolecular hydrogen bonding. The IR properties of these imidazole derivatives have been compared with those of imidazole itself and other imidazole derivatives. A series of complexes of the form $Fe^{III}(TPP)(L)_2SbF_6$, where TPP = tetraphenylporphyrin and L = imidazole or a substituted imidazole, have been synthesized and characterized by visible, electron paramagnetic resonance and IR spectroscopy and cyclic voltammetry in order to evaluate the effects of hydrogen bonding of coordinated imidazole ligands on the properties of iron porphyrin complexes. IR studies demonstrated that imidazole ligands that contain free N-H groups will hydrogen bond to perchlorate ion in solution. Cyclic voltammetric studies of $Fe(TPP)(L)_2SbF_6$ complexes have shown that $E_{1/2}$ of the Fe(III)/Fe(II) couple depends on the pK_a of the ligand and its hydrogen bonding properties. The $E_{1/2}$ values of complexes of imidazoles that form intermolecular hydrogen bonds were shifted to more negative potentials in the presence of excess ligand. By contrast, $E_{1/2}$ values of complexes of cis-methyl urocanate and 1-methyl imidazole were unaffected by excess ligand. The combined evidence of IR and cyclic voltammetry suggests that hydrogen bonding of coordinated imidazoles to uncoordinated imidazoles is of comparable or greater strength than that to *o*-phenanthroline and that both types of hydrogen bond are stronger than that of coordinated imidazole to an ester carbonyl oxygen.

The coordination of the imidazole ring of a histidyl residue to ferric or ferrous hemes has been reported for a variety of hemoproteins. The functions of these proteins are quite varied, ranging from dioxygen transport proteins, such as hemoglobin and myoglobin, to proteins that catalyze oxidations of substrates, such as horseradish peroxidase, and electron-transfer proteins, such as cytochrome b_5. The observation that histidyl imidazole ligands in hemoproteins are usually hydrogen bonded to another group on the protein has led to the hypothesis that such hydrogen bonding might influence the chemical properties of the heme moiety.[2-19]

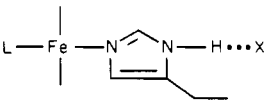

(1) (a) UCLA. (b) Work initiated at Rutgers University, New Brunswick, NJ, and described in: Quinn, R. Ph.D. Dissertation, Rutgers Univeristy, 1983.

(2) Valentine, J. S.; Sheridan, R. P.; Allen, L. C.; Kahn, P. C. *Proc. Natl. Acad. Sci. U.S.A.* **1979**, *76*, 1009-1013.
(3) Nappa, M.; Valentine, J. S.; Snyder, P. A. *J. Am. Chem. Soc.* **1977**, *99*, 5799-5800.
(4) Quinn, R.; Nappa, M.; Valentine, J. S. *J. Am. Chem. Soc.* **1982**, *104*, 2588-2595.
(5) Mohr, P.; Scheler, W.; Schumann, H.; Muller, K. *Eur. J. Biochem.* **1967**, *3*, 158-163.
(6) Swartz, J. C.; Stanford, M. A.; Moy, J. N.; Hoffman, B. M.; Valentine, J. S. *J. Am. Chem. Soc.* **1979**, *101*, 3396-3398.
(7) Stanford, M. A.; Swartz, J. C.; Phillips, T. E.; Hoffman, B. M. *J. Am. Chem. Soc.* **1980**, *102*, 4492-4499.
(8) Stein, P.; Mitchell, M.; Spiro, T. G. *J. Am. Chem. Soc.* **1980**, *102*, 7795-7797.
(9) Scheidt, W. R.; Reed, C. A. *Chem. Rev.* **1981**, *81*, 543-555.

0002-7863/84/1506-4136$01.50/0